Article

Mechanisms of stretch-mediated skin expansion at single-cell resolution

Check for updates

Mariaceleste Aragona[1], Alejandro Sifrim[2,3], Milan Malfait[1], Yura Song[1], Jens Van Herck[2,3], Sophie Dekoninck[1], Souhir Gargouri[1], Gaëlle Lapouge[1], Benjamin Swedlund[1], Christine Dubois[1], Pieter Baatsen[4], Katlijn Vints[4], Seungmin Han[5,6], Fadel Tissir[7], Thierry Voet[2,3], Benjamin D. Simons[5,6,8 ✉] & Cédric Blanpain[1,9 ✉]

The ability of the skin to grow in response to stretching has been exploited in reconstructive surgery[1]. Although the response of epidermal cells to stretching has been studied in vitro[2,3], it remains unclear how mechanical forces affect their behaviour in vivo. Here we develop a mouse model in which the consequences of stretching on skin epidermis can be studied at single-cell resolution. Using a multidisciplinary approach that combines clonal analysis with quantitative modelling and single-cell RNA sequencing, we show that stretching induces skin expansion by creating a transient bias in the renewal activity of epidermal stem cells, while a second subpopulation of basal progenitors remains committed to differentiation. Transcriptional and chromatin profiling identifies how cell states and gene-regulatory networks are modulated by stretching. Using pharmacological inhibitors and mouse mutants, we define the step-by-step mechanisms that control stretch-mediated tissue expansion at single-cell resolution in vivo.

In shaping tissue architecture, cells are subject to mechanical forces arising intrinsically through the cytoskeleton, by cell–cell adhesion, and from the microenvironment through interaction with the extracellular matrix (ECM)[4,5]. Cells sense and respond to these cues via the integrated activation of different signalling pathways. This process of mechanotransduction eventually leads to changes in cell shape, gene expression and cell fate[6]. Although studies have shown that mechanotransduction can dictate cell behaviour in vitro[7], the underlying mechanisms that allow organs to sense and mediate mechanical cues in vivo are only beginning to be revealed.

As the first barrier against the environment, the skin is highly exposed to mechanical stress. The skin must resist and respond to physical insults, as well as adapt its shape and size to maintain vital barrier functions[8].

Mechanical stretch-mediated tissue expansion is a procedure commonly used in plastic surgery to generate extra skin to repair birth defects, remove scars or for breast reconstruction[1]. In this procedure, an inflatable 'skin expander' is inserted below the skin and inflated, causing the expansion of the overlaying skin[1]. During the course of expansion, an excess of cells must be produced. But do all proliferative cells respond equally to stretch, or do subpopulations respond differently? How is mechanosensation linked to gene transcription, and which transcription factors relay mechanical stress to control expansion?

Hydrogel induces mouse skin expansion

To study the cellular and molecular mechanisms that regulate stretch-mediated expansion in vivo, we established a mouse model that mimics the procedure used in humans, in which a self-inflating hydrogel is introduced underneath the skin. The hydrogel is designed to inflate to a predefined shape and size[9]. The 4-ml hydrogel devices expanded rapidly, reaching their maximum volume after one day (Extended Data Fig. 1a–d). During the first two days following expansion, the cell area was increased and cell density decreased, consistent with stretch. After four days, these parameters returned to their homeostatic values, indicating the production of new tissue. At day 2, BrdU incorporation increased twofold, and after day 4, BrdU incorporation decreased progressively, reaching control levels by day 14 after expansion (Fig. 1a–e).

To investigate whether the differentiation rate was affected, we assessed the production of keratin 1+ (Krt1+) and Krt10+ suprabasal cells following expansion. From day 4 onwards, we observed an increase in the number of Krt1+Krt10+ suprabasal layers, demonstrating that stretch-mediated proliferation couples renewing divisions with differentiation (Fig. 1f, g).

During morphogenesis and in in vitro cell culture, stretch is commonly associated with rearrangement of cell–cell junctions[10]. Transmission electron microscopy (TEM) showed that stretch induced intercellular spacing and thicker keratin bundles. Desmosomes and hemidesmosomes remained unchanged (Extended Data Fig. 1e–q). Despite cellular remodelling, the integrity of the skin barrier was maintained, as assessed by transepithelial water loss (TEWL) (Extended Data Fig. 1r). Moreover, the expression of adherens-junction and tight-junction proteins was unchanged (Fig. 1h, i, Extended Data Figs. 1s–w and 2a–d). However, following expansion, the tension-sensitive epitope of α-catenin (a18)[11] was increasingly accessible, and vinculin expression
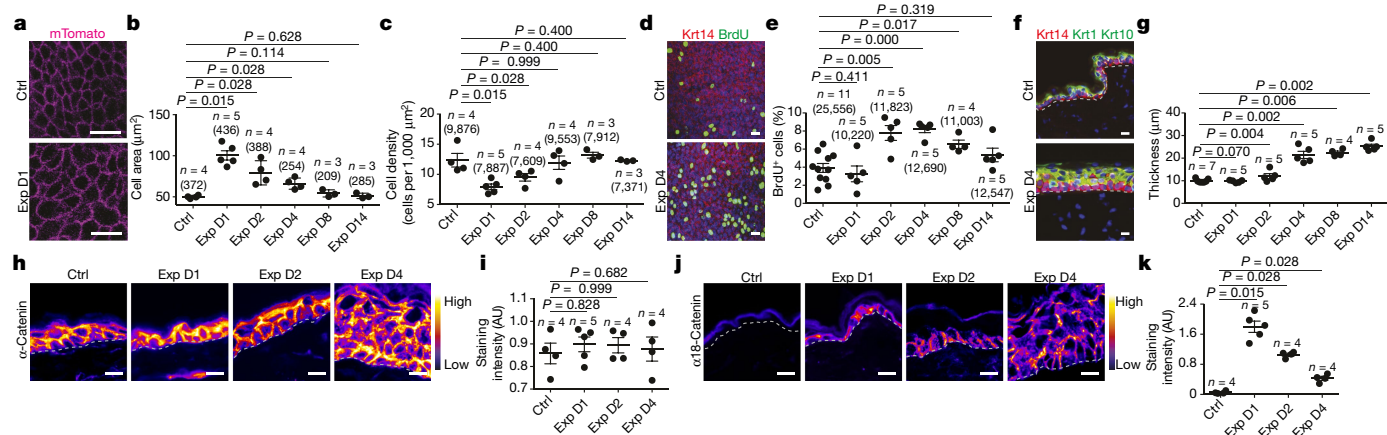
Fig. 1 | Inflated hydrogel mediates skin expansion. a, Membranous signal (pink), from paraformaldehyde-perfused *Rosa26^{mT/mG}* mice in the control condition (Ctrl) and day 1 (D1) of the expansion condition (Exp). Scale bars, 15 μm. **b**, Area of basal cells measured from **a**. **c**, Basal cell density. Number of nuclei per 1,000 μm² (five different independent areas of 40,000 μm² per mouse). **d**, Immunostaining for Krt14 (red), BrdU incorporation (green) and Hoechst staining (nuclei, blue) on whole-mount epidermis. Scale bars, 20 μm. **e**, BrdU-positive cells from **d**. **f**, Immunostaining for Krt14 (red), Krt1 and Krt10 (green), and Hoechst staining (blue) on tissue sections. Scale bars, 20 μm. **g**, Tissue thickness; three independent measurements from at least two sections per mouse. **h**, **j**, Staining of the adherens-junction component α-catenin (**h**) and the α18 tension-sensitive epitope of α-catenin (α18-catenin) (**j**) colour-coded for signal intensity with ImageJ. Protein expression is visualized as a colour gradient with black indicating no expression and yellow indicating maximum expression. Scale bars, 10 μm. **i**, **k**, Average integrated density signal for α-catenin (**i**) and α18-catenin (**k**). Each data point is the average of five measurements per mouse. AU, arbitrary units. In **f**, **h**, **j**, the dashed line indicates the basal lamina. In **b**, **c**, **e**, numbers of cells are in parentheses and *n* = number of mice. Two-tailed Mann–Whitney test; mean per mouse ± s.e.m.

was enriched at the adhesion sites, showing that adherens junctions are remodelled following stretch (Fig. 1j, k, Extended Data Fig. 2e, f).

Although inflammation occurred following expansion, blocking inflammation by dexamethasone administration did not decrease proliferation (Extended Data Fig. 2g–m), suggesting that inflammation is not essential to mediate cell proliferation.

Stretching promotes stem cell renewal

To define the fate dynamics of epidermal cells during stretch-mediated skin expansion, we performed clonal analysis on *Krt14-creER-Rosa^{Confetti}* mice. As described previously[12–14], the steady increase in basal (and total) clone size over the two-week time course was compensated by a decrease in clone persistence, such that the total labelled cell fraction remained constant over time. Furthermore, the clone size distributions showed an exponential-like dependence (Fig. 2a–f, Extended Data Fig. 3a, b), consistent with the dynamics of a single equipotent cell population maintained through population asymmetric self-renewal, as found in other compartments of skin epidermis[12–15].

During stretch-mediated expansion, the average clone size was increased by 3.4-fold in the basal and 6.8-fold in the total cell content, twofold larger than under control conditions. However, in this case, the expansion in basal clone size was not compensated by a decrease in clone persistence (Fig. 2g–k, Methods), indicating that tissue expansion does not simply increase proliferation, but also changes the balance between renewal and differentiation.

To understand the changes that take place in cell fate during expansion, we first considered the homeostatic control condition. Despite its exponential form, detailed inspection of the clone size distribution revealed evidence of a statistically significant bias towards clones bearing an even number of basal cells (65 ± 5% (mean ± s.d.) at day 14), a feature that was also present in the total clone size distribution (57 ± 4% at day 14) (Fig. 2b). Remarkably, this feature was greatly enhanced in 12-*O*-tetradecanoylphorbol-13-acetate (TPA)-treated (Extended Data Fig. 3d–g) and expansion conditions (Fig. 2g, Extended Data Fig. 3h–j), for both basal (80 ± 11% and 84 ± 6%, respectively, at day 14) and total (78 ± 11% and 81 ± 6%, respectively, at day 14) clone size, suggesting that it did not derive from statistical noise or synchrony of division, but

may originate from a niche-like organization of tissue. To develop this idea, we considered an arrangement in which back-skin interfollicular epidermis (IFE) comprised a mosaic of units, each of which hosts two basal cells organized in a stem–progenitor cell-like hierarchy with one basal cell belonging to a renewing (stem cell) compartment and the other a progenitor cell committed to differentiation through terminal division and stratification (Fig. 2l, Supplementary Note). To ensure the prevalence of even cell numbers in clones, we posited that the terminal division and stratification of progenitor cells is compensated predominantly by the asymmetric division of stem cells within the same unit. Further, to account for the expansion of clones beyond two basal cells, we proposed that correlated cell loss and replacement must also occur between neighbouring units. From a fit to the clonal data, we found that this model could predict the distributions of basal and total clone size with a division rate of once per 4.6 days, while around 4 out of 5 divisions of renewing cells result in asymmetric fate outcome, a similar figure to that found in other skin compartments on the basis of a model of intrinsic fate choice[12–16]. Notably, we found that a 'one-progenitor' model based on the correlated differentiation and divisions of neighbours[17] could not reproduce the fine features of the data (Fig. 2l, Extended Data Fig. 3k–p, Supplementary Note).

In common with control and TPA data, the distribution of clone sizes during expansion also showed convergence towards an exponential size dependence (Fig. 2k). We therefore investigated whether a minimal adjustment of the homeostatic model could predict the clone dynamics. Taking as an input the measured proliferation rate on the basis of BrdU incorporation (Fig. 1e), we found that a continuous adjustment of fate imbalance could account for the average clone size increase, as well as the enrichment of even-sized clones, providing evidence that progenitor heterogeneity is conserved during expansion (Extended Data Fig. 4a–g, Supplementary Note).

To further challenge the two-progenitor model and the transient changes in cell fate following skin expansion, we marked cells during division using a BrdU single-pulse-chase assay. We assessed the fate of proliferative cells during stretch, discriminating between daughter cells biased for renewal (Krt14⁺Krt10⁻) and those committed to differentiation (Krt14⁺Krt10⁺). We found that stretching increased the proportion of BrdU⁺Krt14⁺Krt10⁻ cells, consistent with the model, demonstrating
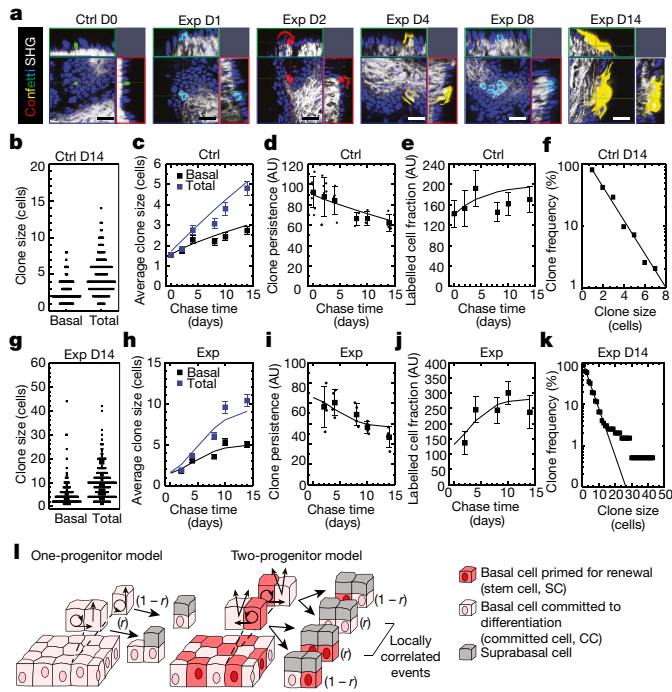
Fig. 2 | Clonal analysis of epidermal stem cells during stretch-mediated skin expansion. a, *Krt14-creER-Rosa^Confetti^* clones (*n* = 4 independent experiments). Second harmonic generation (SHG) imaging visualizes collagen fibres (white). Nuclei stained with 7-aminoactinomycin D (7AAD) (blue). Scale bars, 50 μm. **b–k**, Clonal analysis in control and expansion conditions. **b**, **g**, Distribution of clone sizes at day 14 based on basal and total cell number. **c**, **h**, Average clone size based on basal (black) and total (blue) cell content. **d**, **i**, Clone persistence. **e**, **j**, Average labelled cell fraction. **f**, **k**, Cumulative clone size distribution at day 14 showing an approximate exponential size dependence (lines). In **b–f**: day 0, 115 clones from *n* = 7 mice; day 2, 175 clones from *n* = 7 mice; day 4, 136 clones from *n* = 5 mice; day 8, 159 clones from *n* = 3 mice; day 10, 146 clones from *n* = 3 mice; day 14, 195 clones from *n* = 4 mice. In **g–k**: day 2, 231 clones from *n* = 4 mice; day 4, 197 clones from *n* = 4 mice; day 8, 199 clones from *n* = 4 mice; day 10, 157 clones from *n* = 4 mice; day 14, 199 clones from *n* = 4 mice. **l**, Schematic showing the cellular organization in a one-progenitor model and the proposed two-progenitor model of back-skin IFE. In the two-progenitor model, the epidermis contains renewing stem cells, committed cells and suprabasal cells. In homeostasis, stem cells divide at an average rate λ. This division has a probability of $1 - r$ of an asymmetric fate outcome, leading to the replacement of the partner committed cell, which in turn is lost through terminal division and stratification from the basal layer. The remaining divisions lead to the correlated loss and replacement of renewing cells through symmetric cell divisions. Probability is shown in parentheses. In **c–f**, **h–k**, data are mean ± s.d. In **c–e**, **h–j**, points show data and lines show results of a two-progenitor model (see Supplementary Note).

that expansion promotes an imbalance of the renewing population towards cell duplication (Extended Data Fig. 4h, i).

Molecular features related to stretch

To define the changes in gene expression following expansion, we performed microarray analysis on basal cells isolated by fluorescence-activated cell sorting (FACS) in different conditions (Extended Data Fig. 5a). Genes upregulated in both expanded and TPA conditions comprise those regulating cell cycle, DNA replication, cell survival and cytoskeleton remodelling (Extended Data Fig. 5b, c). Many of these genes are also upregulated during wound healing[18], suggesting that they represent a common transcription program linked to cellular stress and proliferation.

Genes that were preferentially upregulated in the expanded condition were enriched for those related to cell–cell and cell–ECM adhesion,

small GTPase, regulators of the actomyosin cytoskeleton (Fig. 3a) and genes regulating proliferation, including *Egfr*, *Ras*, mitogen-activated protein kinase (MAPK), activator protein 1 (AP1), transcription factors *Junb*, *Fos*, *Fosb* and *Fosl1*, and components of the YAP–TEAD pathway (for example, *Tead1* and the canonical YAP target gene *Cyr61*) (Fig. 3b). Consistently, we found changes in the expression of some of these adhesion and cytoskeleton proteins by immunostaining and FACS analysis (Extended Data Fig. 5d–f).

To unravel the changes in the chromatin landscape that are associated with expansion, we used an assay for transposase-accessible chromatin using sequencing (ATAC-seq) to identify the chromatin regions that were remodelled at day 2 following expansion. To define the transcription factors associated with chromatin remodelling, we performed motif-discovery analyses on the chromatin-remodelled regions. The most frequent motifs associated with open chromatin regions corresponded to AP1, p63, STAT, ETS, CEBP, AP2A and GRHL2 (Fig. 3c, Extended Data Fig. 5g–k, Supplementary Tables 1, 2). Immunostaining confirmed overexpression of members of the AP1 transcription factor family such as FOSL1, FOS and JUN, as well as p63, pSTAT3 and KLF4 in the basal and early suprabasal cells (Fig. 3d–f, Extended Data Fig. 5l–t). These results show that stretch-mediated skin expansion is regulated by the EGFR–Ras–MAPK pathway, leading to the activation of JUN and FOS[19] transcription factors, transcription factors such as p63 that mediate epidermal stem cell renewal[20], as well as transcription factors associated with differentiation, such as CEBP[21], KLF4[22] and GRHL2[23], allowing skin expansion while maintaining skin barrier functions.

scRNA-seq during stretching

To assess whether all basal cells respond equally to stretch, we performed single-cell RNA sequencing (scRNA-seq) on FACS-isolated cells enriched for basal IFE, infundibulum, sebaceous gland and basal upper hair follicle cells in control conditions (*n* = 4,659), after TPA treatment (*n* = 4,342) and following expansion (day 1, *n* = 4,934 and day 4, *n* = 2,716) (Extended Data Fig. 5a). Using graph-based clustering, we identified different subpopulations on the basis of marker gene expression. These different clusters were found in all conditions (Extended Data Fig. 6a–l), and were similar to the clusters described in a previous study[24,25].

On the basis of the clonal analysis, we first questioned whether the scRNA-seq data supported the existence of proliferative heterogeneity in the IFE. When only IFE cells were analysed in control conditions, we identified a population of undifferentiated cells with a stem cell-like signature, a population of proliferative basal committed cells co-expressing basal and early differentiation markers such as Krt1 and Krt10, and a population of non-cycling cells expressing differentiation markers (Fig. 3g). The same IFE populations were found in all conditions, although the proliferative activity of stem cells and committed cells were proportionally increased in expansion and TPA conditions (Fig. 3g, Extended Data Fig. 7a–f, Supplementary Table 3).

In addition, cell states expressing genes associated with stress and hyperproliferation (for example, *Krt6a*, *Sprr1a*, *S100a8*, *Klk10*) were found in the expanded condition (Fig. 3g, Extended Data Fig. 7g). Notably, the stem cell-like 'stretch' cluster appearing on day 1 following expansion–identified by the expression of basal markers (for example, *Krt14*, *Itgb1*) and higher expression of *Ly6a*, *H2-K1*, *Thy1* and *Mt2* (Fig. 3g–i, Extended Data Fig. 7h)–presented increased activity of transcription factors regulating proliferation and immediate early genes (for example, *E2f1* and *Egr1*) as well as AP1 transcription factors (for example, *Fos*, *Junb* and *Jund*), inflammation (for example, *Stat1* and *Stat3*) and commitment or differentiation (for example, *Klf4*), as analysed by SCENIC analysis[26] (Fig. 3j, Extended Data Fig. 8a, Supplementary Tables 4–6), suggesting that only a fraction of basal cells respond transcriptionally to mechanical stress.

To determine the lineage trajectories among the different subpopulations, we performed pseudotemporal ordering of cells using
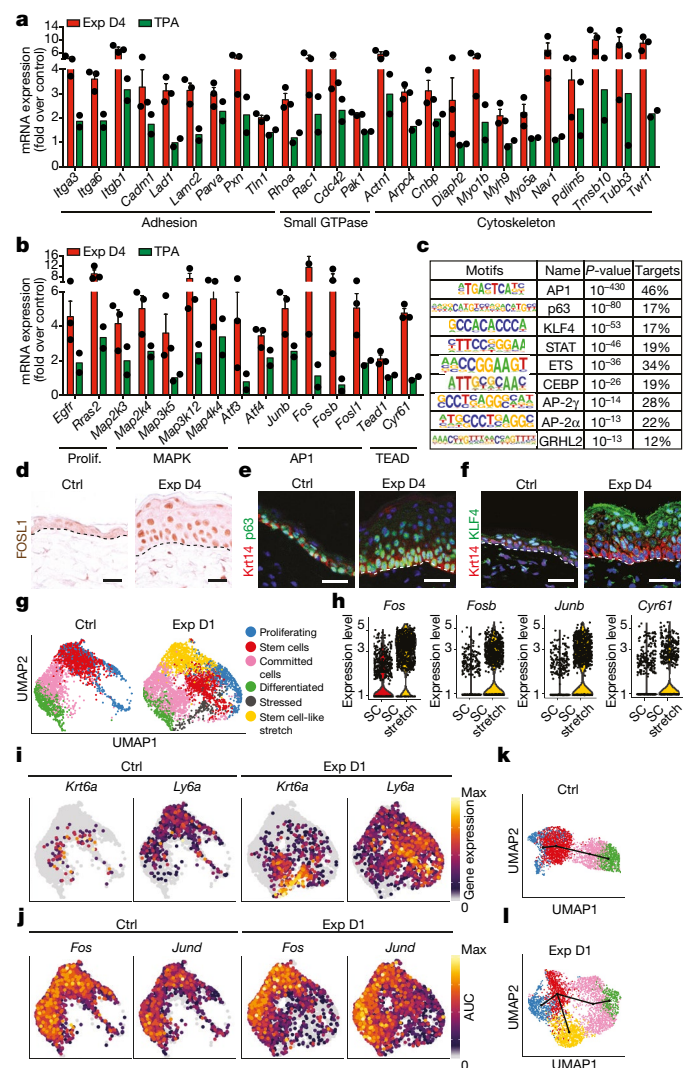
Fig. 3 | Transcriptional and chromatin remodelling associated with stretch-mediated skin expansion. a, **b**, mRNA expression of genes upregulated in day 4 of expansion conditions ($n = 3$) compared with TPA-treated cells ($n = 2$). Bars are mean with s.e.m. of the fold change over the average value of the control ($n = 3$). *Cyr61* is also known as *Ccn1*. Prolif., proliferation. **c**, Transcription factor motifs enriched in the ATAC-seq peaks that were upregulated on day 2 of expansion conditions compared with control ($n = 3,262$ target sequences, 46,200 background sequences) as determined by Homer analysis using known motif search. **d**, Immunohistochemistry for FOSL1. **e**, **f**, Immunofluorescence for p63 (**e**) or KLF4 (**f**) and Krt14, and Hoechst staining. In **d**–**f**, dashed lines delineate the basal lamina. Scale bars, 20 μm. $n = 3$ independent experiments. **g**, Uniform manifold approximation and projection (UMAP) graphic of the clustering analysis for scRNA-seq of the control ($n = 3,142$ cells) and expansion day 1 ($n = 3,756$ cells) IFE projected on an integrated embedding of the dataset. **h**, Violin plots of the indicated genes at expansion day 1 in the stem cell (SC) ($n = 700$ cells) and stem cell-like stretch (SC stretch) ($n = 801$ cells) clusters (see Source Data). **i**, UMAP plots coloured by normalized gene expression values for the indicated genes in the control and expansion day 1 IFE. Gene expression is visualized as a colour gradient with grey indicating no expression (that is, expression below the 50th percentile across each respective sample) and yellow indicating maximum (max) expression. **j**, UMAP plots coloured by the degree of regulon activation for transcription factors differentially activated (area under the curve (AUC) rank-sum test FDR corrected P-value < 0.05) in the different conditions. Colour scaling represents the normalized AUC value of target genes in the regulon being expressed as computed using SCENIC. **k**, **l**, Lineage trajectories (black lines) computed using Slingshot. Clusters are coloured as in **g**. In **i**–**l**, $n = 3,142$ cells (control) and $n = 3,756$ cells (expansion day 1).

Slingshot[27] in control and expansion day 1 conditions. In all conditions, we found a trajectory starting from undifferentiated basal stem cells, passing through the progenitor state, and terminating with the most differentiated cells (Fig. 3k, l, Extended Data Fig. 8b). In expansion day 1 conditions, we resolved another differentiation pathway involving progression through the stress states, delineating the different responses to mechanical cues (Fig. 3l, Extended Data Fig. 8c, d). Together, these data show that stem cells present a rapid and profound response to stretch.

Mechanosensing at adherens junctions

The results of TEM and molecular analysis suggested that stretching induces remodelling of the cytoskeleton, as well as an increase at the transcription level of several genes encoding remodellers of the actomyosin cytoskeleton, such as *Diaph2* and *Diaph3*, and formin-like proteins involved in actin regulation[28] (Fig. 3a, Extended Data Fig. 1e–g, k, Extended Data Fig. 5c, k). To test whether rearrangements of actin organization are essential to mediate the response to stretch, we studied the consequence of *Diaph3* deletion (*Diaph3* conditional knockout (cKO)). The increase in the number of cells presenting F-actin structures on their apical surface on day 1 of expansion was reduced, and no increase in cell proliferation following stretch was observed in *Diaph3* cKO mice (Fig. 4a, Extended Data Fig. 9a–g).

Mechanical stretch has been shown to promote the phosphorylation of myosin II, relaying mechanotransduction in cell lines in vitro[2] and in the *Drosophila* wing disc[29]. Consistently, following conditional ablation of *Myh9*, a key subunit of myosin IIA (*Myh9* cKO), proliferation was not increased in response to stretch (Fig. 4b, Extended Data Fig. 9h–l).

As basal cells sense stretching by remodelling the traction at adherens junctions, we assessed whether *Diaph3* and *Myh9* cKO prevent adhesion remodelling. The accessibility of the α-catenin tension-sensitive epitope and vinculin staining were not increased following stretching in *Diaph3* and *Myh9* cKO mice (Extended Data Fig. 9m–r). Deletion of *Diaph3* and *Myh9* following expansion resulted in the incapacity of the epidermis to adapt to stretch, causing a barrier defect (Fig. 4c).

MEK–ERK–AP1 regulate expansion

Previous studies demonstrated that in vitro mechanical stretching induces proliferation by activation of MEK signalling[30], and that ERK is activated on stress fibres in a myosin II–dependent manner[31]. To assess whether pharmacological inhibition of the MEK–ERK pathway could impair the cellular behaviour following skin stretching, we treated mice with the MEK inhibitors trametinib and pimasertib. Both inhibitors reduced phosphorylation of ERK and resulted in a decrease of cell proliferation and the number of differentiated cells induced by stretching (Extended Data Fig. 10a–g), demonstrating the importance of MEK–ERK–AP1 signalling in the regulation of the stretch response in vivo.

YAP and MAL regulate skin stretching

Previous studies have shown that YES-associated protein 1 (YAP1), the downstream coeffector of Hippo signalling, and megakaryoblastic leukaemia/myocardin-like 1 (MAL, also known as MRTFA or MKL1), the co-factor of serum response factor (SRF), are induced in response to mechanical stimuli[32,33]. In the skin, YAP–TAZ and SRF pathways are essential for epidermal development and wound repair, but are dispensable for homeostasis[34,35]. In vitro studies have demonstrated the role of MAL–SRF in the survival and differentiation of keratinocytes cultured on micropatterned surfaces[36], and that of YAP as a driver of proliferation in stretched cultured cells in vitro[37].

To test whether and when YAP and MAL are activated in vivo, we assessed their subcellular localization at different times during expansion. Whereas YAP and MAL were localized preferentially in the
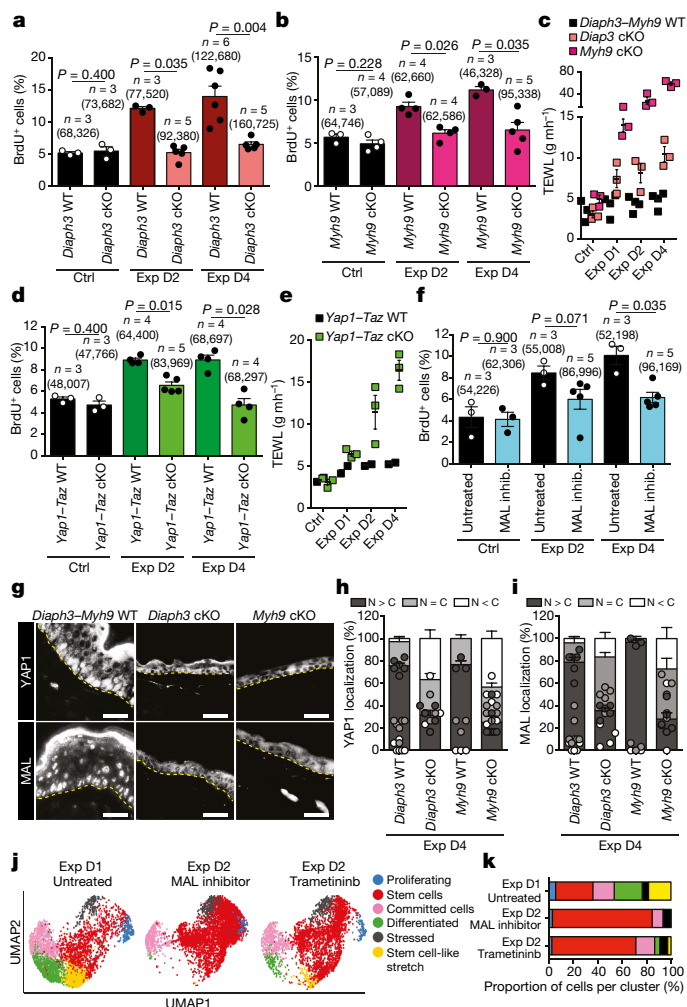
Fig. 4 | Molecular regulation of stretch-mediated skin expansion. a, BrdU-positive cells in control and expansion conditions in *Diaph3* wild-type (WT) or cKO mice. **b**, BrdU-positive cells in control and expansion conditions in *Myh9* WT and cKO mice. **c**, TEWL measurements from *n* = 2 *Diaph3* WT, *n* = 2 *Myh9* WT (black), *n* = 3 *Diaph3* cKO (pink) and *n* = 3 *Myh9* cKO mice (violet). **d**, BrdU-positive cells in control and expansion conditions in *Yap1–Taz* WT or cKO mice. **e**, TEWL measurements from *n* = 2 *Yap1–Taz* WT mice (black) and *n* = 3 *Yap1–Taz* cKO mice (green). **f**, BrdU-positive cells in untreated or treated mice with the MAL inhibitor in control and expansion conditions. **g**, Immunostaining for YAP1 (top) and MAL (bottom) on skin sections of *Diaph3* cKO and *Myh9* cKO mice at expansion day 4. The control images are from a *Diaph3* WT (top) mouse and a *Myh9* WT (bottom) mouse. Dashed lines delineate the basal lamina. Scale bars, 20 μm. **h**, **i**, YAP1 (**h**) and MAL (**i**) subcellular localization in skin sections represented in **g**. Data are mean ± s.e.m. N > C, more protein in nucleus than in cytoplasm; N = C, similar level of protein in nucleus as in cytoplasm; N < C, less protein in nucleus than in cytoplasm. *n* = 150 cells per condition. **j**, UMAP computed on the integrated single-cell RNA-seq dataset coloured for the different cellular clusters in IFE. *n* = 3,869 cells (expansion day 1 untreated); *n* = 4,762 cells (expansion day 2 MAL inhibitor); *n* = 3,254 cells (expansion day 2 trametinib). **k**, Quantification of the cellular clusters in **j**. In **a**–**f**, data are mean ± s.e.m.; *n* = number of mice; total numbers of cells analysed are indicated in parentheses. In **a**, **b**, **f**, two-tailed Mann–Whitney test. In **c**, **e**, each data point represents the average of 30 individual subsequently recorded measurements at the probe head.

cytoplasm in the control, they gradually translocated to the nucleus of basal cells during expansion (Extended Data Fig. 10h–k). These data reveal that YAP and MAL are activated immediately following stretching, but only in a subset of basal cells, similar to AP1 family members (Extended Data Fig. 10l).

To define the functional role of YAP, we induced deletion of *Yap1* and *Taz* specifically in the epidermis (*Yap1–Taz* cKO) and assessed their role during stretch. A significant decrease in BrdU incorporation was observed already by day 2 in *Yap1–Taz* cKO epidermis, as well as a reduction in epidermal thickness (Fig. 4d, Extended Data Fig. 10m–q). In addition, the deletion of *Yap1* and *Taz* following hydrogel expansion caused a barrier defect (Fig. 4e).

To assess the role of MAL activity, we treated the mice immediately after surgery with the pharmacological MAL–SRF inhibitor CCG20397[38], and found a significant decrease of BrdU incorporation and epidermal thickness at day 4 (Fig. 4f, Extended Data Fig. 10r–u). Notably, inhibition of both pathways completely blocked the response to stretch (Extended Data Fig. 11a–d).

As *Diaph3* and *Myh9* control adhesion remodelling upon stretching, we tested whether they act upstream of YAP1 and MAL. In *Diaph3* cKO and *Myh9* cKO epidermis, YAP1 and MAL were not translocated into the nucleus following stretch (Fig. 4g–i, Extended Data Fig. 11e, f), demonstrating the essential role of *Diaph3* and *Myh9* in regulating canonical mechanotransducers. Together, these experiments demonstrate that mechanical stretch couples cytoskeletal contractility with the nuclear effectors of mechanotransduction and stem cell activation in vivo.

scRNA-seq after MEK and MAL inhibition

To define the consequences of the inhibition of the signalling pathways that control stretch-induced proliferation on the cellular heterogeneity and stem cell dynamics in vivo, we performed short-term lineage tracing of basal cells using BrdU pulse-chase combined with immunohistochemistry. The results showed a decrease in renewing divisions (BrdU[+]Krt14^{+}Krt10^{−}) in the *YAP–TAZ* cKO mice and upon inhibition of MAL–SRF or MEK–ERK–AP1 (Extended Data Fig. 11g–l). In addition, short-term genetic lineage tracing in the presence of MAL–SRF or MEK–ERK–AP1 inhibition showed suppression of the increase of clone size following skin expansion (Extended Data Fig. 12a–f). scRNA-seq at day 2 after expansion in the presence of the MEK–ERK–AP1 and MAL–SRF inhibitors showed that, although the inhibition of both pathways led to a similar decrease in cell proliferation, the proportion of cells in different states differed between treatments. Cellular heterogeneity was relatively well conserved following the inhibition of the MEK–ERK–AP1 pathway, whereas the MAL–SRF inhibitor diminished the abundance of stem cells with stress characteristics and decreased the heterogeneity of basal cells (Fig. 4j, k, Extended Data Fig. 12g, h, Supplementary Tables 7–9), suggesting that while the MEK–ERK–AP1 pathway controls only proliferation induced by stretching, the MAL–SRF pathway controls cellular heterogeneity in the basal layer and stretch sensing.

Discussion

We have dissected the cellular and molecular spatiotemporal mechanisms that control the behaviour of epidermal stem cells in response to mechanical stretch. Quantitative modelling of clonal data suggests that proliferation and differentiation of basal cells in back-skin epidermis is spatially and temporally linked, as has been suggested during homeostasis[17,39]. During stretch-mediated skin expansion, a transient shift of stem cell fate towards renewal allows the basal population to expand while differentiation is maintained. These results were supported by results of scRNA-seq, which revealed the existence of different cell states within the basal layer, identifying the molecular signature of stem and committed cells in the mouse back skin, and highlighting the heterogeneous response of basal cells to stretching.

Mechanistically, we found that regulators of the actomyosin cytoskeleton, including formin-like proteins and non-muscle myosin, are essential for sensing skin stretching in vivo, and act upstream of canonical mechanotransducers such as YAP1 and MAL. Of note, the same signalling pathways are activated during embryonic pancreas development[40]

Article

and in the fly notum upon mechanical compression[41], suggesting that these signalling pathways and transcriptional regulators have a conserved role in mechanotransduction across the animal kingdom and between embryonic development and adult tissue regeneration.

Online content

Any methods, additional references, Nature Research reporting summaries, source data, extended data, supplementary information, acknowledgements, peer review information; details of author contributions and competing interests; and statements of data and code availability are available at https://doi.org/10.1038/s41586-020-2555-7.

1. Zöllner, A. M., Holland, M. A., Honda, K. S., Gosain, A. K. & Kuhl, E. Growth on demand: reviewing the mechanobiology of stretched skin. *J. Mech. Behav. Biomed. Mater.* **28**, 495–509 (2013).
2. Le, H. Q. et al. Mechanical regulation of transcription controls Polycomb-mediated gene silencing during lineage commitment. *Nat. Cell Biol.* **18**, 864–875 (2016).
3. Nava, M. M. et al. Heterochromatin-driven nuclear softening protects the genome against mechanical stress-induced damage. *Cell* **181**, 800–817 (2020).
4. Iskratsch, T., Wolfenson, H. & Sheetz, M. P. Appreciating force and shape—the rise of mechanotransduction in cell biology. *Nat. Rev. Mol. Cell Biol.* **15**, 825–833 (2014).
5. LeGoff, L. & Lecuit, T. Mechanical forces and growth in animal tissues. *Cold Spring Harb. Perspect. Biol.* **8**, a019232 (2016).
6. Kirby, T. J. & Lammerding, J. Emerging views of the nucleus as a cellular mechanosensor. *Nat. Cell Biol.* **20**, 373–381 (2018).
7. Vining, K. H. & Mooney, D. J. Mechanical forces direct stem cell behaviour in development and regeneration. *Nat. Rev. Mol. Cell Biol.* **18**, 728–742 (2017).
8. Blanpain, C. & Fuchs, E. Plasticity of epithelial stem cells in tissue regeneration. *Science* **344**, 1242281 (2014).
9. Obdeijn, M. C., Nicolai, J. P. & Werker, P. M. The osmotic tissue expander: a three-year clinical experience. *J. Plast. Reconstr. Aesthet. Surg.* **62**, 1219–1222 (2009).
10. Wickström, S. A. & Niessen, C. M. Cell adhesion and mechanics as drivers of tissue organization and differentiation: local cues for large scale organization. *Curr. Opin. Cell Biol.* **54**, 89–97 (2018).
11. Yonemura, S., Wada, Y., Watanabe, T., Nagafuchi, A. & Shibata, M. α-Catenin as a tension transducer that induces adherens junction development. *Nat. Cell Biol.* **12**, 533–542 (2010).
12. Clayton, E. et al. A single type of progenitor cell maintains normal epidermis. *Nature* **446**, 185–189 (2007).
13. Mascré, G. et al. Distinct contribution of stem and progenitor cells to epidermal maintenance. *Nature* **489**, 257–262 (2012).
14. Sánchez-Danés, A. et al. Defining the clonal dynamics leading to mouse skin tumour initiation. *Nature* **536**, 298–303 (2016).
15. Lim, X. et al. Interfollicular epidermal stem cells self-renew via autocrine Wnt signaling. *Science* **342**, 1226–1230 (2013).
16. Rompolas, P. et al. Spatiotemporal coordination of stem cell commitment during epidermal homeostasis. *Science* **352**, 1471–1474 (2016).
17. Mesa, K. R. et al. Homeostatic epidermal stem cell self-renewal is driven by local differentiation. *Cell Stem Cell* **23**, 677–686 (2018).
18. Aragona, M. et al. Defining stem cell dynamics and migration during wound healing in mouse skin epidermis. *Nat. Commun.* **8**, 14684 (2017).
19. Eferl, R. & Wagner, E. F. AP-1: a double-edged sword in tumorigenesis. *Nat. Rev. Cancer* **3**, 859–868 (2003).
20. Botchkarev, V. A. & Flores, E. R. p53/p63/p73 in the epidermis in health and disease. *Cold Spring Harb. Perspect. Med.* **4**, a015248 (2014).
21. Lopez, R. G. et al. C/EBPα and β couple interfollicular keratinocyte proliferation arrest to commitment and terminal differentiation. *Nat. Cell Biol.* **11**, 1181–1190 (2009).
22. Segre, J. A., Bauer, C. & Fuchs, E. Klf4 is a transcription factor required for establishing the barrier function of the skin. *Nat. Genet.* **22**, 356–360 (1999).
23. Hopkin, A. S. et al. GRHL3/GET1 and trithorax group members collaborate to activate the epidermal progenitor differentiation program. *PLoS Genet.* **8**, e1002829 (2012).
24. Joost, S. et al. Single-cell transcriptomics reveals that differentiation and spatial signatures shape epidermal and hair follicle heterogeneity. *Cell Syst.* **3**, 221–237 (2016).
25. Joost, S. et al. Single-cell transcriptomics of traced epidermal and hair follicle stem cells reveals rapid adaptations during wound healing. *Cell Rep.* **25**, 585–597 (2018).
26. Aibar, S. & Gonzalez-Blas, C. B. SCENIC: single-cell regulatory network inference and clustering. *Nat. Methods* **14**, 1083–1086 (2017).
27. Street, K. et al. Slingshot: cell lineage and pseudotime inference for single-cell transcriptomics. *BMC Genomics* **19**, 477 (2018).
28. Rottner, K., Faix, J., Bogdan, S., Linder, S. & Kerkhoff, E. Actin assembly mechanisms at a glance. *J. Cell Sci.* **130**, 3427–3435 (2017).
29. Duda, M. et al. Polarization of myosin ii refines tissue material properties to buffer mechanical stress. *Dev. Cell* **48**, 245–260 (2019).
30. Yang, K. et al. YAP and ERK mediated mechanical strain-induced cell cycle progression through RhoA and cytoskeletal dynamics in rat growth plate chondrocytes. *J. Orthop. Res.* **34**, 1121–1129 (2016).
31. Hirata, H. et al. Actomyosin bundles serve as a tension sensor and a platform for ERK activation. *EMBO Rep.* **16**, 250–257 (2015).
32. Panciera, T., Azzolin, L., Cordenonsi, M. & Piccolo, S. Mechanobiology of YAP and TAZ in physiology and disease. *Nat. Rev. Mol. Cell Biol.* **18**, 758–770 (2017).
33. Posern, G. & Treisman, R. Actin' together: serum response factor, its cofactors and the link to signal transduction. *Trends Cell Biol.* **16**, 588–596 (2006).
34. Rognoni, E. & Walko, G. The roles of YAP/TAZ and the Hippo pathway in healthy and diseased skin. *Cells* **8**, 411 (2019).
35. Luxenburg, C., Pasolli, H. A., Williams, S. E. & Fuchs, E. Developmental roles for Srf, cortical cytoskeleton and cell shape in epidermal spindle orientation. *Nat. Cell Biol.* **13**, 203–214 (2011).
36. Connelly, J. T. et al. Actin and serum response factor transduce physical cues from the microenvironment to regulate epidermal stem cell fate decisions. *Nat. Cell Biol.* **12**, 711–718 (2010).
37. Aragona, M. et al. A mechanical checkpoint controls multicellular growth through YAP/TAZ regulation by actin-processing factors. *Cell* **154**, 1047–1059 (2013).
38. Whitson, R. J. et al. Noncanonical hedgehog pathway activation through SRF–MKL1 promotes drug resistance in basal cell carcinomas. *Nat. Med.* **24**, 271–281 (2018).
39. Miroshnikova, Y. A. et al. Adhesion forces and cortical tension couple cell proliferation and differentiation to drive epidermal stratification. *Nat. Cell Biol.* **20**, 69–80 (2018).
40. Mamidi, A. et al. Mechanosignalling via integrins directs fate decisions of pancreatic progenitors. *Nature* **564**, 114–118 (2018).
41. Moreno, E., Valon, L., Levillayer, F. & Levayer, R. Competition for space induces cell elimination through compaction-driven ERK downregulation. *Curr. Biol.* **29**, 23–28 (2019).

Methods

Mouse strains

Krt14-creER (ref. [42]) and *Krt14-cre* (ref. [43]) transgenic mice were provided by E. Fuchs (Rockefeller University). *Rosa^Confetti* mice[44] mice were provided by H. Clevers (Hubrecht Institute). *Yap1^fl/fl* and *Taz^fl/fl* mice[45] were obtained from G. Halder (KU Leuven) who received them from R. Johnson at the MD Anderson Cancer Center, Houston. *Diaph3^fl/fl* mice[46] were produced by F. Tissir (UCLouvain) and *Myh9^fl/fl* mice[2] were a gift from S. Wickström (University of Helsinki). *Rosa26^mT/mG* (ref. [47]) mice were provided form I. Migeotte (Université Libre de Bruxelles). Mouse colonies were maintained in a certified animal facility in accordance with European guidelines. The experiments were approved by the local ethical committee (CEBEA) under protocols #604 and #605. The study is compliant with all relevant ethical regulations regarding animal research.

Expander experiments

Mice were anaesthetized (5% xylazine 10% ketamine in PBS) and the dorsal skin was disinfected with 10% iso-Betadine (Meda Pharma), an incision was created in the most caudal part of the dorsal skin to minimize any tension in the wound as the expansion progressed and to maximise the distance from the access wound, to the location of the expander. A subcutaneous pocket was created with forceps and a 4-ml Hemispher Self-inflating tissue expander (Osmed) was placed in the most rostral part under the dorsal skin in proximity of the neck. Stiches were used to close the subcutaneous pocket, to limit the hydrogel movement and to close the access incision.

All analyses were performed in the area on the top of the dome of the hemisphere induced by the skin expander, since this region experiences the highest strain. The hemispherical architecture of the hydrogel has, by its geometric nature, a higher degree of mechanical load at the apex of the hemisphere with isotropic stress[48] and only the skin overlying the very upper part of the hydrogel was studied.

Sample size, randomization and blinding

The sample size was chosen based on previous experience in the laboratory, for each experiment to yield high power to detect specific effects. No statistical methods were used to predetermine sample size. The experiments were not randomized. All animals used were of similar age (60–90 days after birth) and between 28 and 33 g of weight. The investigators were not blinded to allocation during experiments and outcome assessment.

Skin whole-mount

For skin whole-mount confocal microscopy on induced *Krt14-creER-Rosa^Confetti* mice, pieces of entire skin of around 1 cm² were cleared with Sca/eCUBIC-1 and Sca/eCUBIC-2 solutions as described in[49]. The pieces were fixed overnight in 4% paraformaldehyde, incubated 3 days at 37 °C in Sca/eCUBIC-1 solution and incubated at room temperature in Sca/eCUBIC-2 solution for at least 2 days before their analysis. Counterstaining of nuclei was performed with 7AAD (1/1000, Thermo Fisher Scientific). Images were acquired at LiMiF (Université Libre de Bruxelles, Faculté de Médecine, Campus Erasme) on a LSM780NLO confocal system fitted on an Observer Z1 inverted microscope (Zeiss) equipped with a Chameleon Vision II 690-1064 nm multiphoton laser (Coherent Europe) using a Plan Apochromat 20×/0.8 dry objective or LD C Apochromat 40×/1.1 water immersion objective (Zeiss). Spectral images were acquired in lambda mode with a single excitation wavelength at 920 nm and a GaAsp spectral detector (Zeiss). Images 512 by 512 pixels were acquired as a *z*-stack across the thickness of the object. Fluorochromes were separated by linear unmixing using ZEN2012 software (Zeiss). Settings were kept identical for all conditions; this does not apply to the depth (*z* stack) that was adjusted individually to encompass the region of interest. Single plane images were displayed using Zen2012 (Black Edition) software (Zeiss) and exported as uncompressed TIFF images.

Clonal induction in *Krt14-creER-Rosa^Confetti* mice

For lineage tracing experiment, *Krt14-creER-Rosa^Confetti* mice were induced at 2 months of age with Tamoxifen (Sigma) (0.1 mg/g diluted in 10% vol/vol Ethanol and sunflower seed oil, Sigma) by intraperitoneal injection.

Inducing *Yap1*–*Taz* and *Myh9* deletion

For *Yap1-Taz* deletion in *Krt14-creER Yap1^fl/fl Taz^fl/fl* mice and for *Myh9* deletion in *Krt14-creER Myh9^fl/fl* mice, animals received a daily dose of 2.5 mg of tamoxifen (Sigma-Aldrich), for 30 g of body weight, diluted in a mixture of 10% ethanol (VWR) 90% sunflower oil (Sigma-Aldrich) by intraperioneal administration, for 5 consecutive days and every other day after surgery.

Mouse treatments

For TPA treatments, TPA (200 µl of 0.02 mg/ml solution in acetone) was administered daily to shaved mouse back skin for 2 days. To inhibit MEK1/2 activity, mice were treated with Trametinib 2 mg per kg body weight by daily oral gavage, Pimasertib 20 mg per kg body weight daily by oral gavage for at least 7 consecutive days before analysis or as indicated in the figures. To inhibit MAL activity, mice received drug treatment via intraperitoneal injection daily using 100 mg CCG203971 (Cayman Chemical) per kg body weight for 2 or 4 days as indicated in the figures. For the dexamethasone experiments, dexamethasone powder (Sigma) was resuspended at 1 mg ml⁻¹ in ethanol 100% and diluted 5× in sterile PBS. The mice were injected intraperitoneally once per day at the dose of 1 mg kg⁻¹. The treatment started 2 days before the surgery to place the expander and was sustained until the end of the experiment.

Monitoring hydrogel expansion, skin growth, quantification of clone size and persistence

To measure the increase in the hydrogel volume, the height or radius of the expander (*r*) was measured every day (D) from D0 to D14 and the volume calculated as the volume of a half sphere with the formula $V = (2/3) \times \pi r^3$.

To measure basal cell area, whole-mount tissues were obtained from *Rosa26^mT/mG* mice that were fixed by paraformaldehyde perfusion. Images were acquired by two-photon confocal microscopy (40× objective, $z = 1\,\mu m$). Basal cells were identified based on the orthogonal view and if their basal side was in direct contact with the signal of the second harmonic generation. Cell area was measured using ImageJ after manually drawing the contour of each cell revealed by the fluorescence on the membrane on the *Rosa26^mT/mG* mice in the x–y plane.

To define the clone persistence, hair follicles were used as landmarks to calibrate the degree of expansion. During expansion, the total number of hair follicles is not changed, implying that, for an area expansion by a factor ε, the hair follicle density must fall by a factor $1/\varepsilon$. If the area a of each hair follicle remains unchanged during the expansion, for a patch of tissue of area A containing hair follicles spanning an area A_{HF}, the fractional increase in area during the expansion is given by $\varepsilon = A_{HF}^0/A_{HF}$, where A_{HF}^0 is the corresponding area of hair follicles in the control animal. Then, with an average of n clones in an area A, the clonal fractional change in clonal persistence is given by $\varepsilon n/n_0$, where n_0 represents the corresponding clone number in the control animals. For clonal persistence, large areas of tissue (at least 1 cm² per animal) were acquired using the 25× objective and the number of basally attached clones was quantified on the two-photon confocal images in a fixed area of 4 mm² across the different time points.

To quantify the size of the clone, whole-mounts obtained from *Krt14-creER-Rosa^Confetti* mice were imaged by two-photon confocal microscopy. Orthogonal view was used to see in 3 dimensions RFP, YFP, mCFP or nGFP-positive cells and quantify the number of basal and total

Article

cells per clone. Cells were considered as basal when their basal side was in direct contact with the signal of the second harmonic generation.

Epidermal whole-mount and immunostaining

Almost the entire back skin was dissected from the animal, the fat was removed by mechanical scraping with a scalpel and the remaining tissue was cut in pieces of around 2 cm^2 and incubated in PBS/EDTA (20 mM) on a rocking plate at 37 °C for 90 min. Epidermis was separated from the dermis using forceps as an intact sheet and washed 2 times with PBS. Pieces of epidermis were pre-fixed in 4% paraformaldehyde for 1 h at room temperature. Epidermis was rinsed 2 times with PBS for 5 min and conserved in PBS with 0.2% azide at 4 °C. For immunofluorescence staining, entire pieces of epidermis were incubated in blocking buffer (1% BSA, 5% horse serum, 0.8% Triton in PBS) for 3 h at room temperature on a rocking plate (100 rpm). The samples were incubated in primary antibody with anti-Integrin β4 (rat, 1:200, BD Biosciences) overnight at 4 °C. Samples were then washed 3 times in PBS with 0.2% Tween for 1 h and incubated in appropriate secondary antibodies diluted 1:400 in blocking buffer for 1 h at room temperature on the rocking plate. For BrdU staining, samples were incubated in HCl 1M at 37 °C for 35 min, washed with PBS 0.2% tween, stained with anti-BrdU (rat, 1:200, Abcam) in blocking buffer and with appropriate secondary antibody. The following secondary antibodies were used: anti-rat conjugated to AlexaFluor488 (Molecular Probes), to Rhodamine Red-X or to Cy5 (Jackson Immuno Research). Alexa488 or Alexa633 conjugated phalloidin (Thermo Fisher Scientific) was used 1:200 in blocking buffer to visualize F-actin microfilaments. Nuclei were stained in Hoechst solution diluted 1:5000 for 30 min and mounted in DAKO mounting medium supplemented with 2.5% Dabco (Sigma). All confocal images were acquired at room temperature with a LSM780 confocal system fitted on an AxioExaminer Z1 upright microscope equipped with C-Apochromat 40×/1.1 or Plan Apochromat 25×/0.8 water immersion objectives (Zeiss, Iena, Germany). Optical sections 512 × 512 pixels were collected sequentially for each fluorochrome. The datasets generated were merged and displayed with ZEN2012 software (Zeiss).

Histology and immunostaining on sections

Skin epidermis was embedded in OCT and kept at −80 °C. Sections of 6 μm were cut using a CM3050S Leica cryostat (Leica Mycrosystems). After fixation in 4% paraformaldehyde for 10 min at room temperature, tissues were washed 3 times in PBS for 5 min and incubated in blocking buffer (1% BSA, 5% horse serum, 0.2% Triton in PBS) for 1 h at room temperature. Primary antibodies were incubated overnight at 4 °C. Sections were rinsed 3 times in PBS and incubated with secondary antibodies and Hoechst in blocking buffer for 1 h at room temperature. Sections were again washed three times with PBS. The following primary antibodies were used: anti-Krt14 (chicken, 1:20,000, custom batch, Thermo Fisher); anti-Krt1 (rabbit, 1:4,000, Covance/IMTEC, PRB-165P); anti-Krt10 (rabbit, 1:4,000, Covance/IMTEC, PRB-159P); anti-c-JUN (rabbit, 1:200; Proteintech, 24909-1-AP); anti-p63 (rabbit, 1:100 Abcam, ab124762); anti-KLF4 (rabbit, 1:100 Abcam, ab129473); anti-pSTAT3 (rabbit, 1:100 Cell signaling, 9145); anti-YAP1 (rabbit, 1:100 Proteintech, 13584-1-AP); anti-MAL (rabbit, 1:100, Sigma, HPA030782); anti-α-catenin (rabbit, 1:1000 Sigma, C2081); anti-α18-catenin (rat monoclonal, 1:20,000, a gift form A. Nagafuchi, Kumamoto University); anti-Vinculin (mouse, 1:200 Millipore MAB3574); anti-p120-catenin (rabbit, 1:1000 Invitrogen PA5-82545); anti-E-cadherin (rat, 1:500, ebioscience 14-3249-82); anti-ZO-1(rabbit, 1:200 Invitrogen 61-7300); anti-Claudin-1 (rat, 1:100 Thermo Scientific 51-9000); anti-Paxillin (rabbit, 1:100 Abcam 32084); anti-CD45 (rat, 1:500, BD Biosciences 553081); anti-CD68 (rabbit, 1:100 Abcam ab125212).

The following secondary antibodies were used diluted to 1:400: anti-mouse, anti-rat, anti-rabbit, anti-chicken conjugated to Alexa Fluor 488 (Molecular Probes), to rhodamine Red-X (Jackson Immuneresearch) or to Cy5 (Jackson Immunoresearch). Nuclei were stained in Hoechst solution (1:2000) and slides were mounted in DAKO mounting medium supplemented with 2.5% Dabco (Sigma). All images of section immunostaining were acquired using the Axio Imager M1 Microscope, the AxioCamMR3 or MrC5 camera and using the Axiovision software (Carl Zeiss). Acquisitions were performed at room temperature using 20× numerical aperture (NA) 0.4 (Carl Zeiss).

Immunofluorescence intensity measurements

To quantify the intensity of the immunostaining for proteins at the adherens junctions (α-catenin, α18-catenin, β-catenin, p120-catenin) and Paxillin, ImageJ was used to measure the integrated density, a well-established method of measuring fluorescence intensity that accounts for differences in area[50] of the signal in the basal layer of the skin (labelled by Krt14). To quantify the integrated density of the signal of the tight junction proteins ZO-1 and Claudin-1, the measurements were taken on the upper suprabasal layers. Images are shown with the pseudo-colour Fire from ImageJ after they have been contrasted equally and background was uniformly removed with Adobe Photoshop.

Immunohistochemistry

For staining on paraffin sections, 4μm paraffin sections were deparaffinized and rehydrated. Antigen unmasking was performed for 20 min at 98 °C in citrate buffer (pH 6) using the PT module. Endogenous peroxidase was blocked using 3% H$_2$O$_2$ (Merck) in methanol for 10 min at room temperature. Endogenous avidin and biotin were blocked using the Endogenous Blocking kit (Invitrogen) for 20 min at room temperature. Nonspecific antigen blocking was performed using blocking buffer. Rabbit anti-YAP (1:200, Santa Cruz Biotechnology, sc-15407), rabbit anti-TAZ (1:100, Sigma-Aldrich, HPA007415), rabbit anti-cFOS (1:100, Proteintech, 26192-1-AP), rabbit anti-MYH9 (1:500, Sigma, HPA001644), rabbit anti-pERK (1:200, Cell signaling, 4370S) were incubated overnight at 4 °C. For anti-FOSL1 (1:500, Santa Cruz Biotechnology, sc-28310) and anti-β-catenin (mouse, 1:1,000 Abcam ab6301) tissue were also blocked with Mouse on Mouse (M.O.M.) Blocking Reagent (Vector Laboratories). Anti-rabbit biotinylated with blocking buffer, anti-mouse biotinylated with blocking buffer, Standard ABC kit, and ImmPACT DAB (Vector Laboratories) were used for the detection of horseradish peroxidase (HRP) activity. Slides were then dehydrated and mounted using SafeMount (Labonord).

Proliferation experiments

For BrdU experiments, mice were injected with a single intraperitoneal injection of BrdU (50 mg/kg in PBS) at different time points and killed 4 h after. For the quantification an area of at least 1.5 mm^2 per mouse was analysed with Zen2012 (Black Edition) software (Zeiss) to determine the percentage of BrdU-positive cells.

Trans-epithelial water loss measurement

TEWL was measured on back skin of isoflurane-sedated mice using a TEWA meter TM210 (Courage and Khazaka). Every measurement represents the average of 30 individual subsequently recorded measurements at the probe head.

Transmission electron microscopy

The skin was cut into pieces of approximately 1 cm^2 and pre-fixed 2 h at room temperature in the fixative solution composed of 4% paraformaldehyde (Sigma-Aldrich) and 2.5% of electron microscopy grade glutaraldehyde (Sigma-Aldrich) diluted in 0.1M cacodylate buffer pH 7.4 (Sigma). Subsequently the pieces were cut again to reach an approximate size of 1 mm^2 and immersed in the fixative solution at 4 °C overnight. After washing 6 times for 10 min in 0.1 M cacodylate buffer on ice under slow rotation, the samples were post-fixed for 2 h in 2% osmium tetroxide and again washed 6 times for 10 min in water. Samples were then stained with 0.5% uranyl acetate overnight at 4 °C in the dark. The following day the samples were washed 6 times for

10 min in water and incubated with lead aspartate (Walton's lead aspartate composed of 0.02 M lead nitrate in 0.03 M sodium aspartate pH 5.5) for 45 min at 60 °C in the dark. After the samples were washed in water (6 × 10 min) and dehydrated in a graded ethanol series of 50, 70 and 90% on ice (20 min steps) and 100% ethanol (3 × 20 min) before being placed in propylene oxide (2 × 20 min). The samples were infiltrated in a mixture of 2:1 propylene oxide/epoxy resin (Agar) for 1 h at room temperature and in a mixture of 1:1 propylene oxide/epoxy resin for 1 h at room temperature before being left overnight in 1:2 propylene oxide/epoxy resin mixture with open lid to allow evaporation of propylene oxide. The next morning, samples were placed in 100% epoxy resin that was changed every 2 h and embedded at the end of the day in 100% fresh resin. They were incubated overnight at 45 °C and at 60 °C for 2 days to allow polymerization. Samples were processed into 50–70 nm ultrathin sections using a Leica Ultracut UCT ultra-microtome. Micrographs were taken in a JEOL JEM1400 transmission electron microscope equipped with an Olympus Quemesa 11 Mp camera at 80 kV accelerating voltage.

Dissociation of epidermal cells, cell sorting and microarray analysis

The mice were shaved with an electric shaver, the back skin was dissected, and the fat and underlying subcutis were removed with a scalpel. The samples were placed in 0.25% Trypsin (Gibco, Thermo Fisher Scientific) in DMEM (Gibco, Thermo Fisher Scientific) and 2mM EDTA (Thermo Fisher Scientific) overnight at 4 °C. The epidermis was separated from the dermis and the trypsin was neutralized by adding DMEM medium supplemented with 2% Chelex Fetal Calf Serum (FCS). Samples were filtrated on 70 and 40 µm filters (Falcon). Single-cell suspensions were incubated in 2% FCS/PBS with primary antibodies for 30 min on ice, protected from the light, with shaking every 10 min. Primary antibodies were washed with 2% FCS/PBS and cells incubated for 30 min in APC-conjugated streptavidin (BD Biosciences), on ice, with shaking every 10 min. Living epidermal cells were gated by forward scatter, side scatter and negative staining for Hoechst dye. Basal IFE and infundibulum cells were stained using PE-conjugated anti-α6-integrin (clone GoH3, 1:200, ebioscience) or FITC- conjugated anti-α6-integrin (clone GoH3, 1:200, ebioscience) and bulge cells were stained with biotinylated CD34 (clone RAM34; 1:50, BD Biosciences). Basal cells from the IFE were targeted using CD34 negative and α6 integrin positive gating. The geometric mean fluorescence intensity of Itgβ1 (FITC-coniugated anti-β1-integrin, 1:100, BD Bioscience 555005) and Itga2 (PE-coniugated anti-α2-integrin, 1:100, BD Bioscience 553858) was measured on the α6-integrin^{high}CD34$^-$ population.

Fluorescence-activated cell sorting analysis was performed using FACSAria I at high pressure (70 psi) and FACSDiva software (BD Biosciences). Sorted cells (300 cells per sample) were harvested directly in 45 µl of lysis buffer (20 mM DTT, 10 mM Tris.HCl ph 7.4, 0.5% SDS, 0.5 µg/µl proteinase K). Samples were then lysed at 65 °C for 15 min and frozen. RNA isolation, amplification and microarray were performed in the Functional Genomics Core, Barcelona. cDNA synthesis, library preparation and amplification were performed as described in[51]. Microarrays were then performed on Mouse Genome 430 p.m. strip Affymetrix array. The data were normalized using RMA algorithm. The entire procedure was repeated in three technical independent samples for the control and the EXP D4 condition and in two technical independent samples for the TPA treatment. Genetic signatures were obtained by considering genes presenting a fold change greater or smaller than 2 or −2, respectively in both biological replicates.

RNA extraction and quantitative PCR

Fresh-frozen pieces of mouse skin were reduced to powder with a mortar and RNA extraction was then carried out with the RNAeasy Microkit from Quiagen according to the manufacturer's protocol. Purified RNA was used to synthesize the first-strand complementary DNA using SuperScript II (Invitrogen) with random hexamers (Roche).

Quantitative PCR analyses were carried out with Light Cycler 96 (Roche). Primers used: TNFα-5′: ACCACGCTCTTCTGTCTACT, TNFα-3′: AGGAGG TTGACTTTCTCCTG, IFNγ-5′: TCAAGTGGCATAGATGTGGAA, IFNγ-3′: CACTCGGATGAGCTCATTGA, CCL2-5′: CAGGTCCCTGTCATGCTTCT, CCL2-3′: GTCAGCACAGACCTCTCTCT, CCL5-5′: ACCATGAAGATCTCTG CAGC, CCL5-3′: TGAACCCACTTCTTCTCTGG. Normalizers: HPRT-5′: GCAGTACAGCCCCAAAATGG, HPRT-3′: TCCAACAAAGTCTGGCCTGT, Gapdh-5′: CGTGTTCCTACCCCCAATGT, Gapdh-3′: GTGTAGCCCAAG ATGCCCTT.

ATAC sequencing

For ATAC-seq, 100000 sorted basal cells were collected in 1 ml PBS supplemented with 3% FBS at 4 °C. Cells were centrifuged and cell pellets were resuspended in 100 µl lysis buffer (TrisHCl 10 mM, NaCl 10 mM, MgCl2 3 mM, Igepal 0.1%) and centrifuged at 500g for 25 min at 4 °C. Supernatant was carefully discarded and nuclei were resuspended in 50 µl reaction buffer (Tn5 transposase 2.5 µl, TD buffer 22.5 µl, from Nextera DNA sample preparation kit, Illumina, and 25 µl H$_2$0). The reaction was performed at 37 °C for 30 min and was stopped by adding 5 µl clean up buffer (NaCl 900 mM, EDTA 300 mM). DNA was purified using the MiniElute purification kit (QIAGEN) following the manufacturer's protocol. DNA libraries were PCR amplified (Nextera DNA Sample Preparation Kit, Illumina), and size selected from 200 to 800 bp (BluePippin, Sage Sciences), following the manufacturer's recommendations.

ATAC-seq analysis

Adaptor sequences were removed with TrimmomaticPE using options 'HEADCROP:10 CROP:70 ILLUMINACLIP:adaptor.file:2:30:10 LEADING:3 TRAILING:3 SLIDINGWINDOW:4:15 MINLEN:60'. ATAC−seq paired-end reads were then aligned to mouse genome Grcm38 using Bowtie2 (v.2.2.6)[52] using options '-X 2000−fr−very-sensitive− no-discordant−no-unal−no-mixed −non-deterministic'. Mitochondrial reads, reads from unmapped or random counting and reads with a mapping quality <20 were removed using SAMtools[53]. Duplicate reads were removed by Picard tools (http://broadinstitute.github.io/picard/).

Peak calling was performed on each individual sample by MACS2 (v.2.1.0.20151222)[54] using options '-f BAMPE -g mm −nomodel− call-summits -B −SPMR', q-value 0.0001. Peaks from the different subpopulations were merged for downstream analysis.

Reads counts of each merged peak for each individual sample were calculated by HTSeq-count[55] using options '-f bam -r pos -m intersection-nonempty'. These counts were normalized for one million mapped reads in merged peaks and fold-change was calculated compared to control. Peaks were associated to genes with GREAT software[56] with the following parameters: 5.0 kb in proximal upstream, 1.0 kb in proximal downstream and 100.0 kb in distal. For most of the analysis, only peaks annotated to at least one gene were kept.

Differential peaks are defined as peaks having at least a twofold change compared to control and being called peak in the expanded condition and contain at least 3 reads per million.

De novo motif search was performed using findMotifsGenome.pl program in HOMER software[57] searching for motifs of 6 to 12 bp in a region of 500 bp around the peak centre.

Single-cell RNA sequencing

Single basal cells from the back skin were FACS sorted (Integrin alpha 6 high, Cd34 negative) after dissociation. 6000 cells were loaded onto each channel of the Chromium Single Cell 3′ microfluidic chips (V2-chemistry, PN-120232, 10X Genomics) and barcoded with a 10X Chromium controller according to the manufacturer's recommendations (10X Genomics). RNA from the barcoded cells was subsequently reverse transcribed, followed by amplification, shearing 5′ adaptor and sample index attachment. The Libraries were prepared using the Chromium Single Cell 3′ Library Kit (V2-chemistry, PN-120233, 10X

Article

Genomics) and sequenced on an Illumina HiSeq 4000 (paired-end 100bp reads).

Single-cell transcriptomic data analysis

Sequencing reads were aligned and annotated with the mm10-1.2.0 reference dataset as provided by 10X Genomics and demultiplexed using CellRanger (v.2.1.1) with default parameters. Further downstream analyses were carried out individually for each of the four samples (*CTRL*, *EXP. D1*, *EXP.D4* and *TPA*). Quality control was performed using the *scater* R package (v.1.10.0)[58]. For each sample, all of the cells passed the following criteria: had more than 4,000 UMI counts, showed expression of more than 1,500 unique genes and had less than 10% UMI counts belonging to mitochondrial sequences. Read counts were normalized using deconvoluted cell-specific size factors with the *scran* R package (v.1.10.2)[59]. Cell-cycle phases were assigned using the *cyclone* function from *scran*[60]. Dimensional reduction and clustering were performed using the *Seurat* R package (v.3.1.1). A PCA for each sample was calculated using the scaled expression data of the most variable genes (identified as outliers on a mean/variability plot, implemented in the *FindVariableGenes* function from *Seurat*). To remove unwanted sources of variability caused by differences in cycling stages but retaining the distinction between cycling and non-cycling cells, the differences between S-phase and GS/M-phase scores (determined by *cyclone*) were regressed out during scaling (by setting the *vars.to.regress* parameter of the *ScaleData* function in *Seurat*). UMAP[61] calculation and graph-based clustering were done for each sample using the appropriate functions from *Seurat* (default parameters) with the respective PCA results as input. Different values of the *resolution* parameter were tested for the clustering. We set the final resolution to 0.6 (after testing a range from 0.3–1.2) first in the control sample, and then applied the same parameters to the other samples. Given that the obtained clustering sensitivity for a given resolution is dependent on the number of cells of that subpopulation in each respective sample, we swept over the same range of resolutions for the other samples, to assure the presence/absence of described clusters in all samples. This resolution best reflected the biological heterogeneity that emerged from the lineage tracing and the analysis of the clonal data, identifying a progenitor population (characterized by intermediate levels of *Krt5*, *Krt14*, *Krt1* and *Krt10*) that emerged as an intermediate cluster between the stem cells (that expressed high levels of *Krt14*, *Krt15* and integrins) and the differentiated population (highly enriched in *Krt1* and *Krt10*). A Wilcoxon rank-sum test was used to define marker genes for each cluster. Benjamini–Hochberg FDR correction for potential cluster marker genes across all samples ($n = 10,651$) using the p.adjust method in R and only markers expressed in at least 25% of cells of the cluster, having an average log-fold change of at least 0.25 were reported. Differentially expressed genes and regulons between the CTRL SCs and EXP D1 STRETCH SCs and SCs clusters were computed as two-sided Wilcoxon ranked sum tests using the *FindMarkers* function in *Seurat* and p-values were FDR adjusted for the total number of comparisons ($n = 542$ and $n = 571$ respectively). Pseudotime ordering of cells was calculated using *slingshot* (v.1.1.0)[27]. We checked the robustness of the resulting trajectories by performing the analysis on PCA and UMAP reductions and also on downsampled subsets of the data to half the dataset size, these different reductions and permutations did not affect the described trajectories. Gene regulatory network analysis was performed using SCENIC[26] with default parameters. Differentially activated regulons for each cluster were determined by performing a Wilcoxon rank-sum test on the normalized regulon AUC values of cells in the various clusters, *p*-values were FDR-adjusted using the Benjamini–Hochberg method and regulons with an adjusted *p*-value less than 0.05 were considered differentially activated. For visualization purposes we integrated the CTRL, EXP D1, EXP D2 and TPA samples using the *Seurat* package's standard CCA-MNN based data integration workflow. Feature selection was performed using the *FindVariableFeatures* function fom *Seurat* with default parameters, selecting the 2,000 most variable genes. Canonical correlation analysis (CCA) followed by integration anchors selection was then performed on the selected features using the *FindIntegrationAnchors* function from *Seurat*, taking the first 20 dimensions from the CCA into account, as described by the *Seurat* authors[62]. These anchors were then used to integrate the data with the *IntegrateData* function.

To compare the single-cell RNA-seq data from the treated EXP D2 samples (*EXP D2-Trametinib* and *EXP D2-MAL inhibitor*), data integration was performed with the *EXP D1* sample following the approach implemented in *Seurat*[62]. The samples with the treatments were sequenced at a different time point than the *EXP D1* sample and had in general lower UMI count distributions. Therefore, the UMI counts matrix of the *EXP D1* sample was first downsampled, using the *downsampleMatrix* function from the *DropletUtils* package (https://bioconductor.org/packages/release/bioc/html/DropletUtils.html), such that its total number of counts was the same as the average of the total number of counts of the treatment samples. QC filtering and pre-processing was then performed as described before for each individual sample before integration. Further downstream analyses such as dimensionality reduction and clustering were all performed as described before using the integrated data. Cell-cycle phase prediction and differential expression analysis were performed on the uncorrected data to avoid interfering with the underlying distribution assumptions of these statistical methods. Cluster annotation was mainly performed by comparing the overlap of the new clusters of the integrated data with the original cell type annotations of the *EXP D1* sample and by studying the expression of known marker genes. Differentially expressed genes and regulons between the EXP D1 SCs and the EXP D2 SC clusters were computed as two-sided Wilcoxon ranked sum tests using the *FindMarkers* function in *Seurat* and p-values were FDR adjusted for the total number of comparisons ($n = 13,786$ and $n = 758$ respectively). Subpopulations that are not associated with the IFE (infundibulum and sebaceous gland) were removed for the final analysis.

Statistical analysis

Two-tailed Student's *t*-test, two-tailed Mann–Whitney *U*-test and Wilcoxon signed-rank test were performed using GraphPad Prism v.7.00 for Mac (GraphPad Software). Bar graphs and dot plots were generated by GraphPad Prism and show mean ± s.e.m. unless otherwise indicated.

Reporting summary

Further information on research design is available in the Nature Research Reporting Summary linked to this paper.

Data availability

Data associated with this study have been deposited in the NCBI Gene Expression Omnibus under accession numbers GSE126231, GSE126734 and GSE146637, respectively, for the microarray, ATAC-seq and scRNA-seq. Data supporting the findings of this study are available within the Article (and its Supplementary Information files). Source data are provided with this paper.

Code availability

Custom computer code and algorithms used to generate results that are reported in the paper are available within the article (and its Supplementary Information files) and from the corresponding authors on reasonable request. The code used for the modelling of the clonal data has been deposited in GitHub (available at https://github.com/BenSimonsLab/Aragona_Nature_2020).

42. Vasioukhin, V., Degenstein, L., Wise, B. & Fuchs, E. The magical touch: genome targeting in epidermal stem cells induced by tamoxifen application to mouse skin. *Proc. Natl Acad. Sci. USA* **96**, 8551–8556 (1999).

43. Vasioukhin, V., Bauer, C., Degenstein, L., Wise, B. & Fuchs, E. Hyperproliferation and defects in epithelial polarity upon conditional ablation of alpha-catenin in skin. *Cell* **104**, 605–617 (2001).
44. Snippert, H. J. et al. Intestinal crypt homeostasis results from neutral competition between symmetrically dividing Lgr5 stem cells. *Cell* **143**, 134–144 (2010).
45. Xin, M. et al. Hippo pathway effector Yap promotes cardiac regeneration. *Proc. Natl Acad. Sci. USA* **110**, 13839–13844 (2013).
46. Damiani, D., Goffinet, A. M., Alberts, A. & Tissir, F. Lack of Diaph3 relaxes the spindle checkpoint causing the loss of neural progenitors. *Nat. Commun.* **7**, 13509 (2016).
47. Muzumdar, M. D., Tasic, B., Miyamichi, K., Li, L. & Luo, L. A global double-fluorescent Cre reporter mouse. *Genesis* **45**, 593–605 (2007).
48. Tepole, A. B., Gart, M., Purnell, C. A., Gosain, A. K. & Kuhl, E. The incompatibility of living systems: characterizing growth-induced incompatibilities in skin. *Ann. Biomed. Eng.* **44**, 1734–1752 (2016).
49. Susaki, E. A. et al. Whole-brain imaging with single-cell resolution using chemical cocktails and computational analysis. *Cell* **157**, 726–739 (2014).
50. Ellis, S. J. et al. Distinct modes of cell competition shape mammalian tissue morphogenesis. *Nature* **569**, 497–502 (2019).
51. Gonzalez-Roca, E. et al. Accurate expression profiling of very small cell populations. *PLoS ONE* **5**, e14418 (2010).
52. Langmead, B. & Salzberg, S. L. Fast gapped-read alignment with Bowtie 2. *Nat. Methods* **9**, 357–359 (2012).
53. Li, H. et al. The Sequence Alignment/Map format and SAMtools. *Bioinformatics* **25**, 2078–2079 (2009).
54. Zhang, Y. et al. Model-based analysis of ChIP-Seq (MACS). *Genome Biol.* **9**, R137 (2008).
55. Anders, S., Pyl, P. T. & Huber, W. HTSeq—a Python framework to work with high-throughput sequencing data. *Bioinformatics* **31**, 166–169 (2015).
56. McLean, C. Y. et al. GREAT improves functional interpretation of cis-regulatory regions. *Nat. Biotechnol.* **28**, 495–501 (2010).
57. Heinz, S. et al. Simple combinations of lineage-determining transcription factors prime cis-regulatory elements required for macrophage and B cell identities. *Mol. Cell* **38**, 576–589 (2010).
58. McCarthy, D. J., Campbell, K. R., Lun, A. T. & Wills, Q. F. Scater: pre-processing, quality control, normalization and visualization of single-cell RNA-seq data in R. *Bioinformatics* **33**, 1179–1186 (2017).
59. Lun, A. T., Bach, K. & Marioni, J. C. Pooling across cells to normalize single-cell RNA sequencing data with many zero counts. *Genome Biol.* **17**, 75 (2016).
60. Scialdone, A. et al. Computational assignment of cell-cycle stage from single-cell transcriptome data. *Methods* **85**, 54–61 (2015).
61. Becht, E. et al. Dimensionality reduction for visualizing single-cell data using UMAP. *Nat. Biotechnol.* **37**, 38–44 (2019).
62. Stuart, T. et al. Comprehensive integration of single-cell data. *Cell* **177**, 1888–1902 (2019).

Author contributions M.A. and C.B. designed the experiments. M.A., B.D.S and C.B. performed data analysis. M.M., A.S., J.V.H. and T.V. performed scRNA-seq and analysis. S.H. helped with data analysis. S.D., S.G. and G.L. helped with experiments and animal follow-up. Y.S. and B.S. performed ATAC-seq analysis. C.D. helped with FACS. P.B. and K.V. performed TEM. F.T. contributed with genetic tools. M.A., B.D.S. and C.B. wrote the manuscript. All authors read and approved the final manuscript.

**Competing interests** The authors declare no competing interests.

Additional information
Supplementary information is available for this paper at https://doi.org/10.1038/s41586-020-2555-7.
Correspondence and requests for materials should be addressed to B.D.S. or C.B.
Peer review information *Nature* thanks Carien Niessen, Nathan Salomonis and the other, anonymous, reviewer(s) for their contribution to the peer review of this work.
**Reprints and permissions information** is available at http://www.nature.com/reprints.

Article
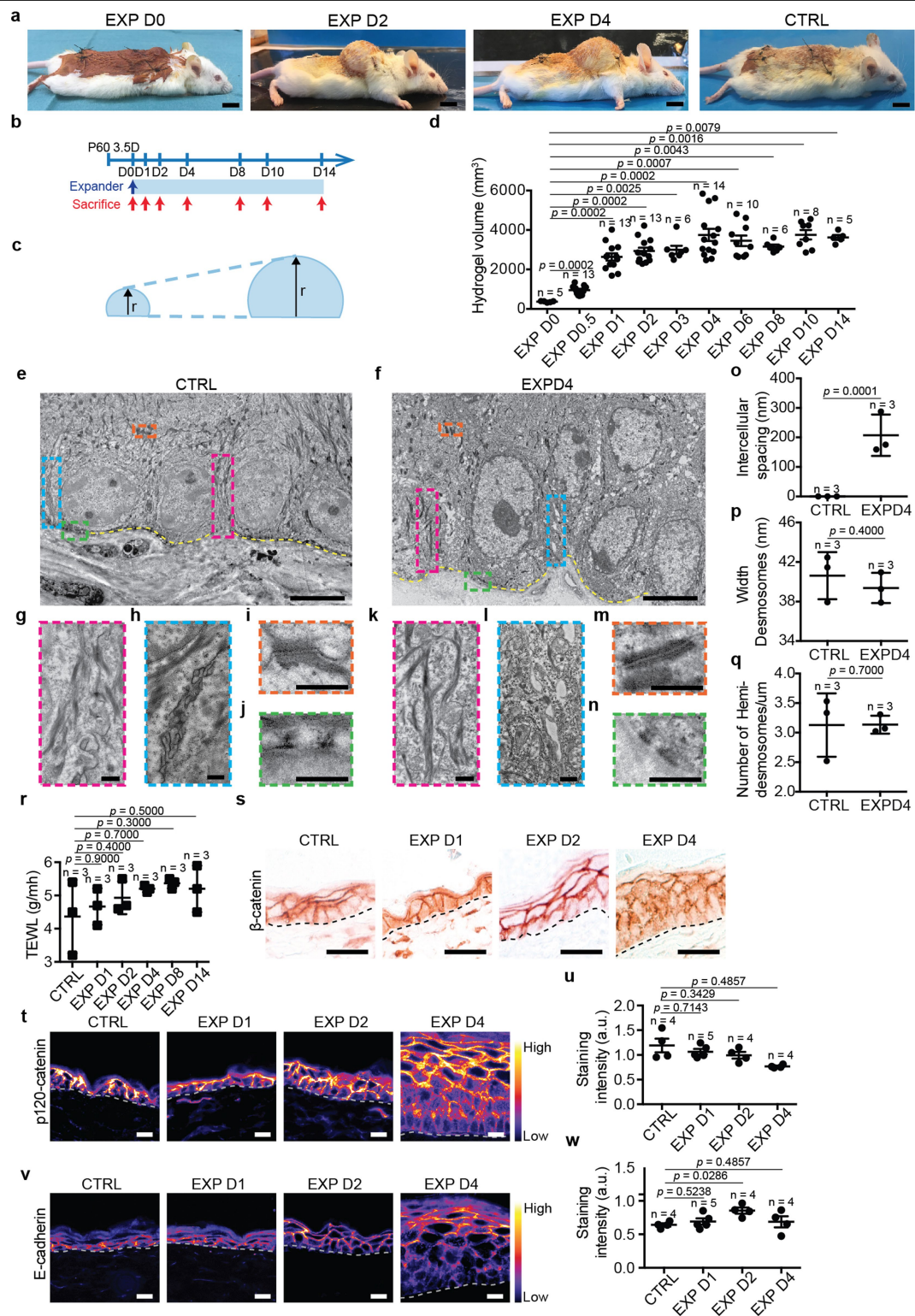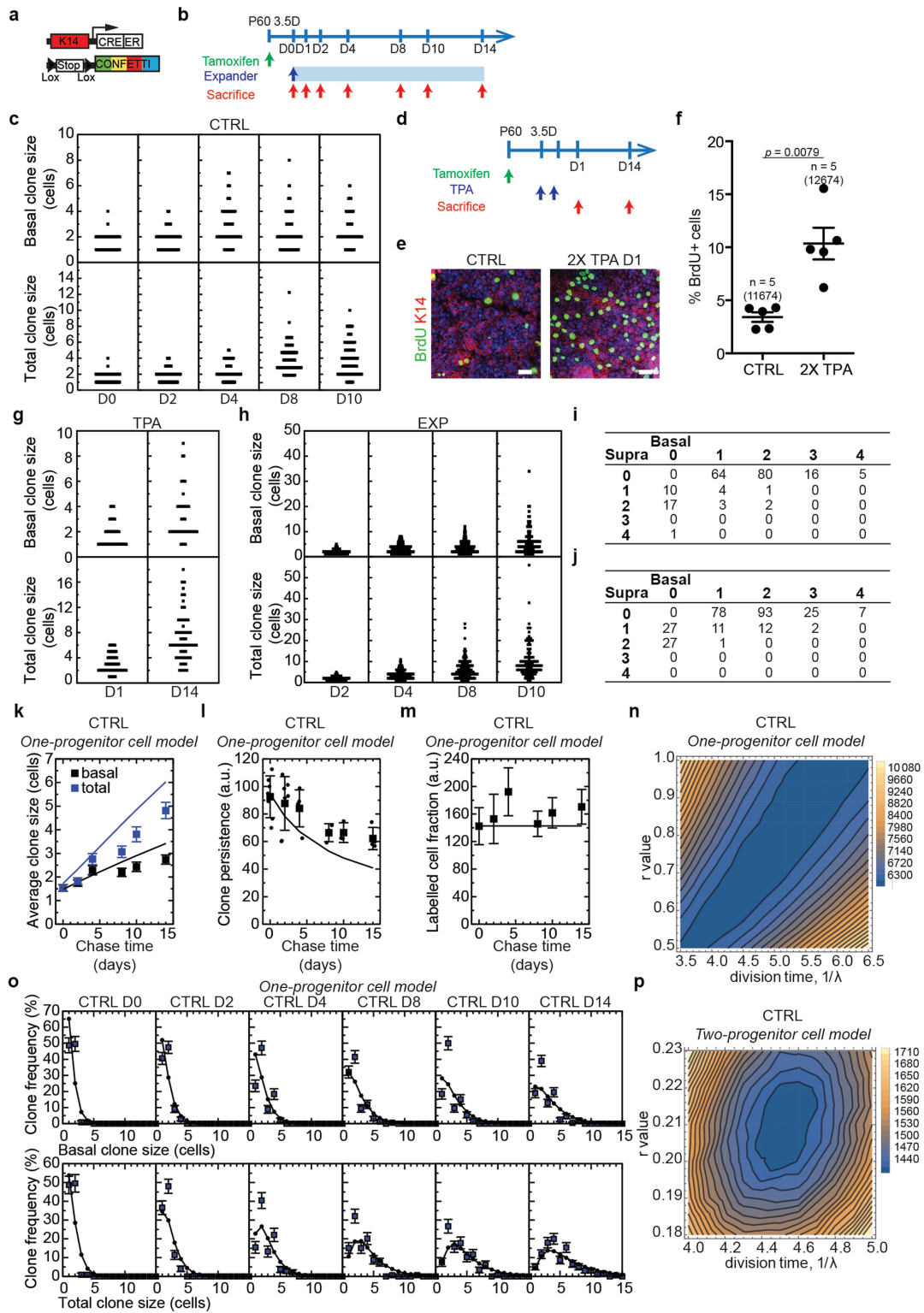

Extended Data Fig. 1 | See next page for caption.

Extended Data Fig. 1 | A mouse model of mechanical stretch-mediated skin expansion. a, Representative photographs of mice with the skin expander immediately after surgery at day (D) D0, D2, D4 and in control (CTRL) condition. Scale bars, 10 mm. The device was implanted on the back skin of the animals, close to the neck where the rigidity of the proximate cervical spines allows the hydrogel to stretch the skin during the inflation of the expander. Control mice were operated upon similarly but without introducing the hydrogel. **b**, Timeline of the experiment. CD1 mice were operated to place the expander and followed over time. **c**, Scheme showing the growth of the hydrogel. The arrows indicate the radius of the hemisphere. **d**, Hydrogel volume (measured by the height of the hydrogel and calculated as the volume of a hemisphere, see Methods, $n = 5$ D0, $n = 13$ D0.5, $n = 13$ D1, $n = 13$ D2, $n = 7$ D3, $n = 13$ D4, $n = 10$ D6, $n = 6$ D8, $n = 8$ D10, $n = 5$ D14 mice). **e–n**, TEM of ultrathin sections of control (**e**, **g–j**) and expanded (**f**, **k–n**) epidermis. In **e** and **f**, dashed yellow lines denote dermal-epidermal boundary and boxed area in pink, cerulean, orange and green are shown at higher magnification, respectively, in **g** and **k**, **h** and **l**, **i** and **m**, **j** and **n**. Scale bars, 5 µm. **g**, **k**, Keratin bundles. **h**, **l**, Ultrastructural analysis of cell–cell adhesion. **i**, **m**, Desmosomes.

j, **n**, Hemidesmodomes. **o**, Quantification of the intercellular spacing on images as in **h** and **l**. Wilcoxon signed-rank test, two-sided. **p**, Quantification of the width of the desmosomes as in **i** and **m**. **q**, Quantification of the width of the number of hemidesmosomes per µm in **j** and **n**. **r**, TEWL measurements from $n = 3$ CD1 mice in CTRL and at different time point during expansion. **s**, Immunohistochemistry for the adherens junctions (AJ) component β-catenin, $n = 3$ independent experiments. **t**, **v**, Representative images of AJ component p120-catenin (**t**) and E-cadherin (**v**) colour-coded for the signal intensity with ImageJ. Protein expression is visualized as a colour gradient going from black to yellow, with black as indicator of no expression and yellow as indicator of maximal expression. Scale bars, 10 µm. **u**, **w**, Quantification of the average integrated density signal for p120-catenin (**u**) and E-cadherin (**w**). Each data point is the average of 3 sections per mouse ($n = 3$ mice per condition). **o–q**, The quantifications are made on $n = 3$ different animals per condition on 10 different samples per mouse and represented as mean + s.e.m. **g–n**, Scale bars, 500 nm. **d**, **p–r**, **u**, **w**, Two-tailed Mann–Whitney test, mean + s.e.m.
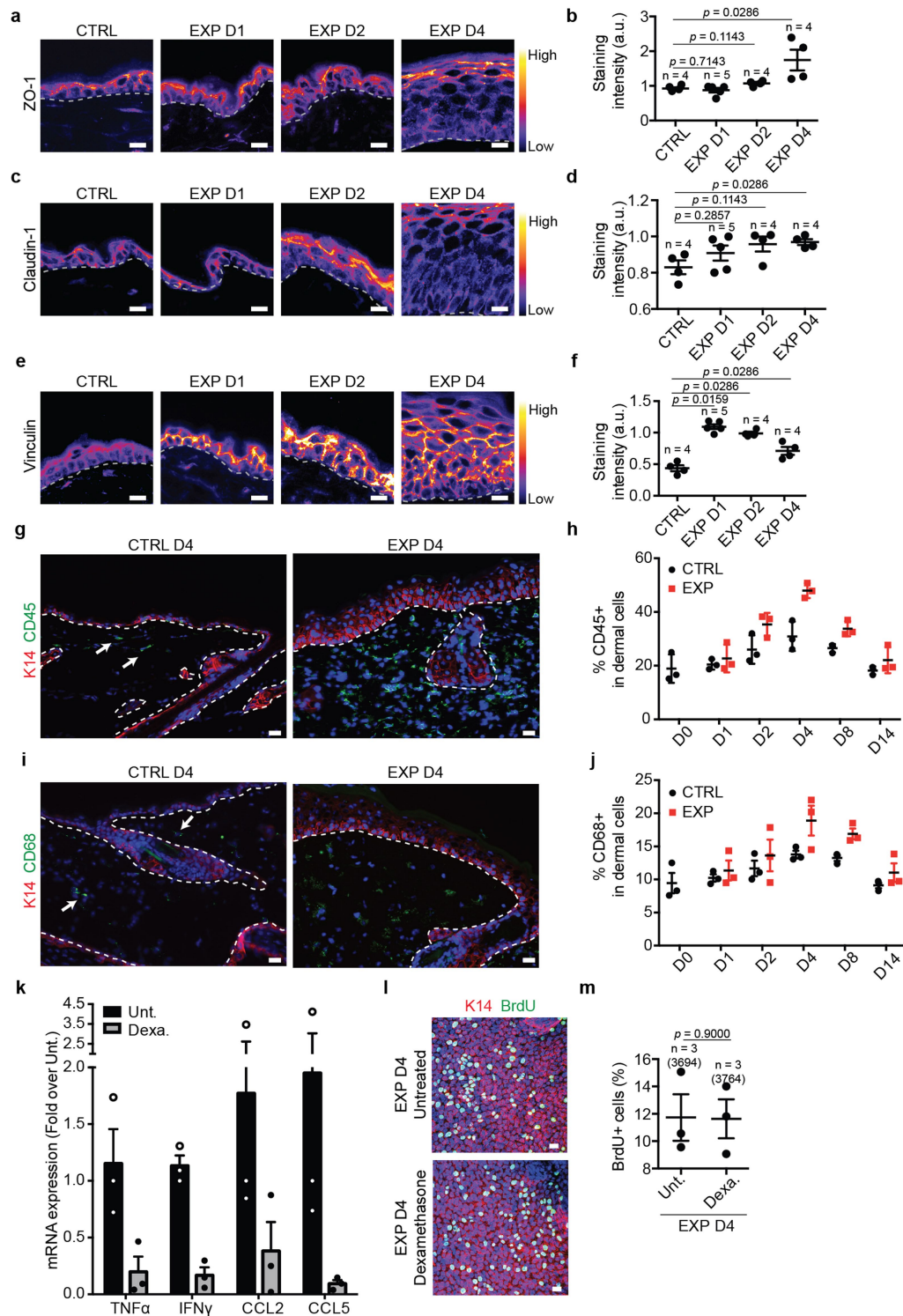
Extended Data Fig. 2 | Adhesion remodelling and inflammatory response during stretch-mediated skin expansion. a, **c**, **e**, Representative images of the tight junction (TJ) components ZO-1 (**a**) and Claudin-1 (**c**) and of Vinculin (**e**) colour-coded for the signal intensity with ImageJ. Protein expression is visualized as a colour gradient going from black to yellow, with black as indicator of no expression and yellow as indicator of maximal expression. Scale bars, 10 μm. **b**, **d**, **f**, Quantification of the average integrated density signal for ZO-1 (**b**), Claudin-1 (**d**) and Vinculin (**f**). The number of mice per condition is indicated. **g**, **i**, Immunostaining for K14 (red), inflammatory cells stained with CD45 (**g**) and macrophages stained with CD68 (**i**) (green) and Hoechst for nuclei (blue) on tissue sections. Scale bars, 10 μm. White arrows indicate positive cells, $n = 3$ independent experiments. **h**, **j**, Percentage of CD45 (**h**) and

CD68 (**j**) positive cells on the total dermal cells quantified based on the nuclear staining, $n = 3$ mice per condition, mean per mouse + s.e.m. **k**, mRNA expression analysis for the indicated gene in Untreated (Unt., black) skin and skin treated with Dexamethasone (Dexa., grey). Fold change is expressed compared to one Unt. sample, $n = 3$ mice per condition, mean per mouse + s.e.m. **l**, Maximum intensity projection of confocal pictures showing immunostaining for K14 (red), BrdU (green) and Hoechst for nuclei (blue) 4 h following BrdU administration on whole mount epidermis. Scale bars, 10 μm. **m**, Proportion of basal cells that are BrdU positive ($n = 3,694$ cells counted from 3 mice for Untreated and $n = 3,764$ cells from 3 mice for the Dexamethasone treatment). **a**, **c**, **e**, **g**, **i**, Dashed lines indicate the basal lamina. **b**, **d**, **f**, **m**, Two-tailed Mann–Whitney test, mean per mouse + s.e.m.
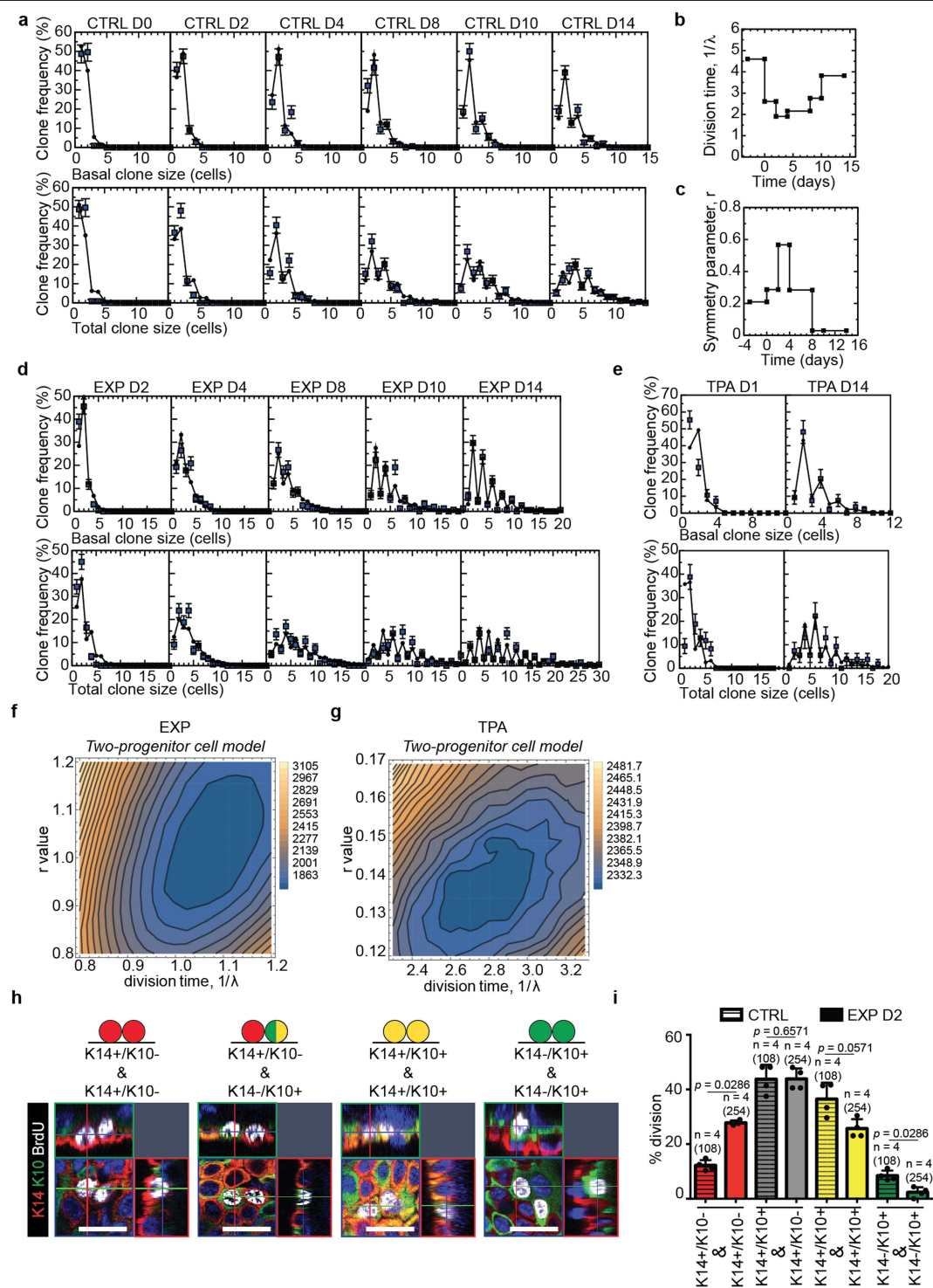
Extended Data Fig. 3 | See next page for caption.

Article

Extended Data Fig. 3 | Clonal analysis of epidermal stem cells during homeostasis, TPA treatment and stretch-mediated skin expansion.
a, Genetic labelling strategy used to trace K14 IFE SC in the back skin during homeostasis and stretch-mediated tissue expansion. **b**, Timeline of the experiment. *Krt14-creER-Rosa*^{Confetti} mice were induced with Tamoxifen at 2 months of age and operated upon 3.5 days after to place the expander. The samples were collected 0, 1, 2, 4, 8, 10 and 14 days after surgery. **c**, Raw distribution of clone size taken from mouse back skin under normal homeostatic conditions (CTRL) at different time points based on basal (top) and total (bottom) cell number. Note that times are calibrated so that the "day 0" time-point is acquired 3.5 days after Tamoxifen injection, requiring effective chase times to be calibrated accordingly, see **b**. D0: 115 clones from n = 7 mice; D2: 175 clones from n = 7 mice; D4: 136 clones from n = 5 mice; D8: 159 clones from n = 3 mice; D10: 146 clones from n = 3 mice. **d**, Time line of the experiment to perform clonal tracing upon TPA treatment. *Krt14-creER-Rosa*^{Confetti} mice were induced with Tamoxifen at 2 months of age and after 3.5 days topically treated with 12-*O*-Tetradecanoylphorbol-13-acetate (TPA) for 2 consecutive days. The samples were collected 1 and 14 days after treatment. **e**, Maximum intensity projection of representative confocal pictures showing immunostaining for K14 (red) and BrdU (green) following BrdU administration on whole mount epidermis form mice treated with TPA or with vehicle (CTRL). Hoechst nuclear staining in blue. Scale bars, 20 μm. **f**, Percentage of BrdU positive cells in control and mice treated with TPA at D1 (n = 5). Two-tailed Mann–Whitney test, mean + s.e.m. **g**, Raw distribution of clone size taken from mouse back skin during TPA treatment (TPA) based on basal (top) and total (bottom) cell number. D1: 85 clones from n = 4 mice; D14: 54 clones from n = 5 mice. **h**, Raw distribution of clone size taken from mouse back skin under stretch-mediated tissue expansion (EXP) at different time points based on basal (top) and total (bottom) cell number. As with control, note that times are calibrated so that the "day 0" time-point is acquired 3.5 days after Tamoxifen injection, requiring effective chase times to be calibrated accordingly. D2: 231 clones from n = 4 mice; D4: 197 clones from n = 4 mice; D8: 199 clones from n = 4 mice; D10: 157 clones from n = 4 mice. **i**, Table showing the abundance (raw counts) of clones by their basal and suprabasal cell composition from the CTRL D2 condition (that is, 5 days post-induction), n = 203 clones from 7 mice. **j**, Table showing the abundance (raw counts) of clones by their basal and suprabasal cell composition from the EXPD2 condition, n = 283 clones from 4 mice. **k**, Fit of the one-progenitor model to the average size of persisting clones in control conditions based on the basal (black) and total (blue) cell content. Points show data and lines are the results of the fit to a one-compartment model (see Methods). **l**, **m**, **o**, Fit to the one-progenitor cell model. Clone persistence (**l**), labelled cell fraction (**m**), and the distribution of basal (upper) and total (lower) clone size (**o**). Points show data and lines are the results of the fit to a one-progenitor model. **k**–**m**, **o**, D0: 115 clones from n = 7 mice; D2: 175 clones from n = 7 mice; D4: 136 clones from n = 5 mice; D8: 159 clones from n = 3 mice; D10: 146 clones from n = 3 mice; D14: 195 clones from n = 4 mice. **n**, **p**, Sensitivity analysis of the model fits depicted as a map of the total square-differences of the experimental basal/total clone size data and the respective model predictions as a function of the average division time, $1/\lambda$, and the degree of imbalance towards stem cell loss/replacement, r, (see Methods). Panel **n** shows the results of one-progenitor model and the CTRL data, **p** shows the results of two-progenitor model and the CTRL data. These results show both the enhanced accuracy of the two-progenitor model over the one-progenitor model, despite involving the same number of fit parameters. **k**–**m**, Mean + s.d. **o**, Mean + s.e.m.
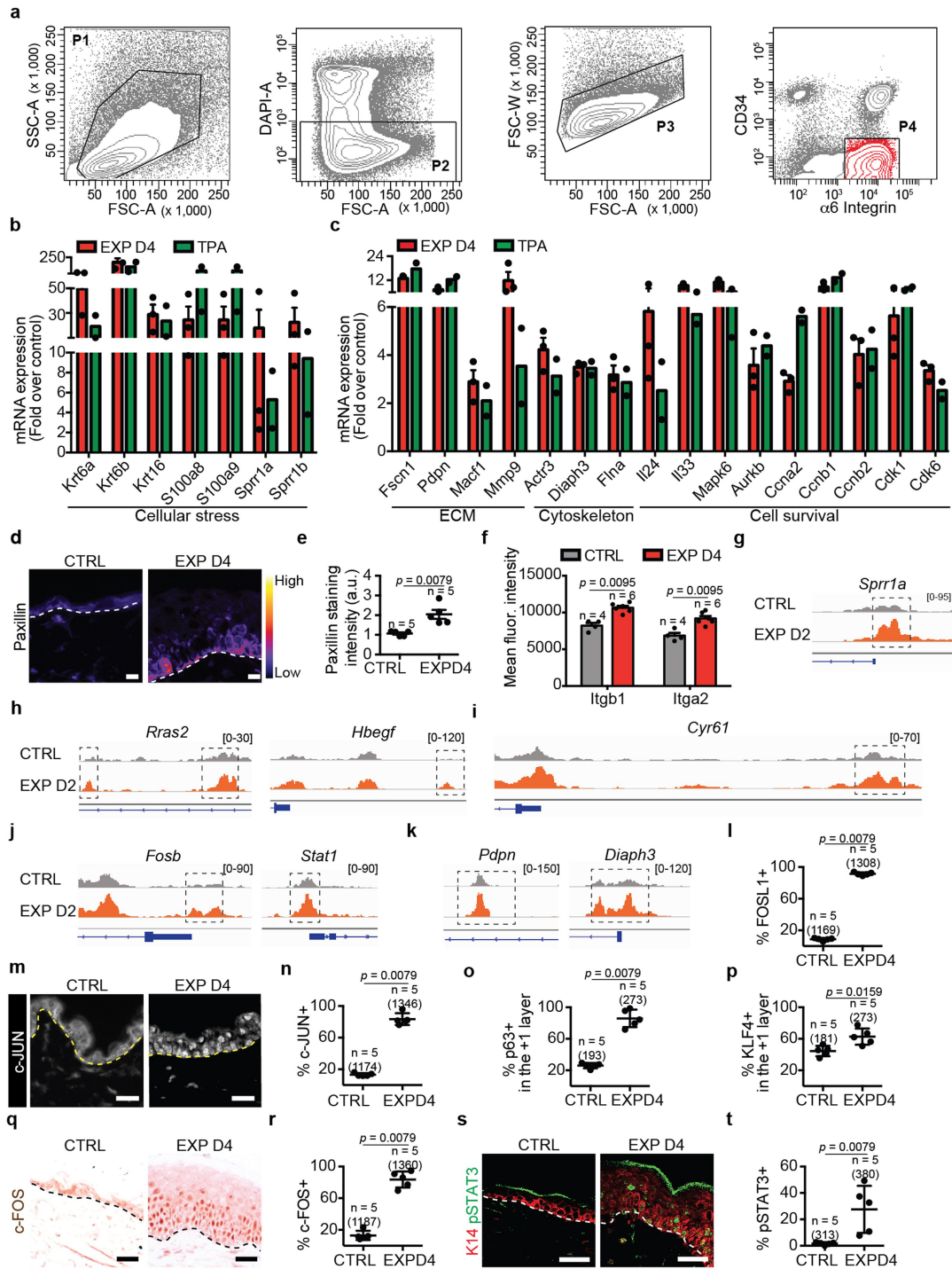
Extended Data Fig. 4 | See next page for caption.

Article

Extended Data Fig. 4 | Fit of the data to the two-progenitor model. a, Fit of the model to the clone size distribution under homeostatic control conditions. Note that, with $1/\lambda = 4.6$ days and $r = 0.21$, the model faithfully reproduces both the exponential-like clone size distribution and the predominance of clones bearing an even number of basal and total cell numbers. Mean + s.e.m. D0: $n = 115$ clones from 7 mice; D2: $n = 175$ clones from 7 mice; D4: $n = 136$ clones from 5 mice; D8: $n = 159$ clones from 3 mice; D10: $n = 146$ clones from 3 mice; D14: $n = 195$ clones from 4 mice. **b**, Change of division time ($1/\lambda$) during stretch-mediated expansion as parameterised from the measured rate of BrdU incorporation, Fig. 1e. **c**, Change in the probability of symmetric division (parameter, r) during stretch-mediated skin expansion obtained from a fit of the two-compartment model to the clone size data (for details, see Supplementary Note). **d**, Corresponding fit of the two-compartment model to the clone size distribution during stretch-mediated expansion. The model accurately reproduces both the exponential-like clone size distribution and the predominance of clones bearing an even number of basal and total cell numbers. Notably, the sharp increase in even-sized clones at long times can only be recovered by limiting the frequency of renewing divisions well below that of the control value. Mean + s.e.m. D2: $n = 231$ clones from 4 mice; D4: $n = 197$ clones from 4 mice; D8: $n = 199$ clones from 4 mice; D10: $n = 157$ clones from 4 mice. **e**, Fit of the model to the clone size distribution at D14 under TPA treatment. Note that with $1/\lambda = 2.3$ days and $r = 0.15$, the model faithfully reproduces both the exponential-like clone size distribution and the predominance of clones bearing an even number of basal and total cell numbers. Mean + s.e.m. D1: $n = 85$ clones from 4 mice; D14: $n = 54$ clones from 5 mice. **f, g**, Sensitivity analysis of the model fits depicted as a map of the total square-differences of the experimental basal/total clone size data and the respective model predictions as a function of the average division time, $1/\lambda$, and the degree of imbalance towards stem cell loss/replacement, r, (see Methods). Panels (**f**) shows the results of the results of two-progenitor model and the EXP data, and (**g**) shows the results of two-progenitor model and the TPA data. For the EXP data (**f**), we have imposed the measured relative variation of the proliferation rate (as inferred from BrdU incorporation) (Fig. 1e and panel (**b**)) and an inferred relative variation of the r parameter as obtained from a model fit (**c**), while the two parameters in panel (**f**) represent variation in the net rates. **h**, Representative orthogonal confocal sections immunostained for Krt14 (red), Krt10 (green) following short-term BrdU (white) incorporation identifying cells biased for renewal (Krt14$^+$Krt10$^-$), cells primed for differentiation (Krt14$^+$Krt10$^+$) and differentiated cells (Krt14$^-$Krt10$^+$). **i**, Percentage of the type of divisions in CTRL (108 divisions from $n = 4$ mice) and EXP D2 (254 divisions from $n = 4$ mice) based on short-term BrdU tracing and staining as in **h**. Two-tailed Mann–Whitney test, mean + s.e.m.

Extended Data Fig. 5 | See next page for caption.

Article

Extended Data Fig. 5 | Genetic signature of TPA-treated and expanded epidermis. a, Representative FACS plots showing the strategy used to isolate basal cells. Single living cells were gated by debris exclusion (P1), DAPI exclusion (P2), doublet elimination (P3) and basal IFE Integrin-α6^{high} CD34^{neg} cell were sorted (P4). $n = 10$ independent experiments. **b, c**, mRNA expression of genes that were upregulated in basal cells at EXP D4 ($n = 3$) and in cells treated with TPA ($n = 2$). These genes are related to a generic stress signature (**b**), regulating ECM remodelling and cytoskeleton, important for cell survival and cell cycle (**c**). Bars are mean with s.e.m. **d**, Representative images of Paxillin immunostaining colour-coded for the signal intensity with ImageJ. Protein expression is visualized as a colour gradient going from black to yellow with black as indicator of no expression and yellow as indicator of maximal expression. Scale bars, 10 μm **e**, Quantification of the average integrated density signal for Paxillin as in **d**. Each data point is the average of 3 sections per mouse ($n = 3$ mice per condition). **f**, Geometric mean fluorescence intensity for the indicated integrin in CTRL (grey, $n = 4$ mice) and EXP D4 (red, $n = 6$ mice) from FACS analysis of basal IFE Integrin-α6^{high} CD34^{neg} cells. **g–k**, ATAC-seq profiles showing increasing accessibility of chromatin regions that are specifically remodelled during mechanical expansion (CTRL in grey and EXP D2 in orange). **l**, Quantification of the number of cells FOSL1+ in the basal layer related to Fig. 3d. **m**, Immunostaining on skin sections for JUN (white) in control and EXP D4. **n**, Quantification of the number of cells JUN+ in the basal layer related to **m. o**, Quantification of the number of cells p63+ in the +1 layer related to Fig. 3e. **p**, Quantification of the number of cells KLF4+ in the +1 layer related to Fig. 3f. **q**, Immunohistochemistry on paraffin sections for c-FOS in control and EXP D4. Scale bars, 20 μm. **r**, Quantification of the number of cells c-FOSL+ in the basal layer related to **q. s**, Immunofluorescence on tissue sections for pSTAT3 in green and K14 (red) to identified the epidermis. Scale bars, 20 μm. **t**, Quantification of the number of cells positive for pSTAT3 in the basal layer related to **s. l, n, o, p, r, t**, 3 sections quantified per n = number of mice and total number of cells indicated in parentheses **d, m, q, s**, Dashed lines delineate the basal lamina. **e, f, l, n–p, r, t**, Two-tailed Mann–Whitney test, Mean + s.e.m.
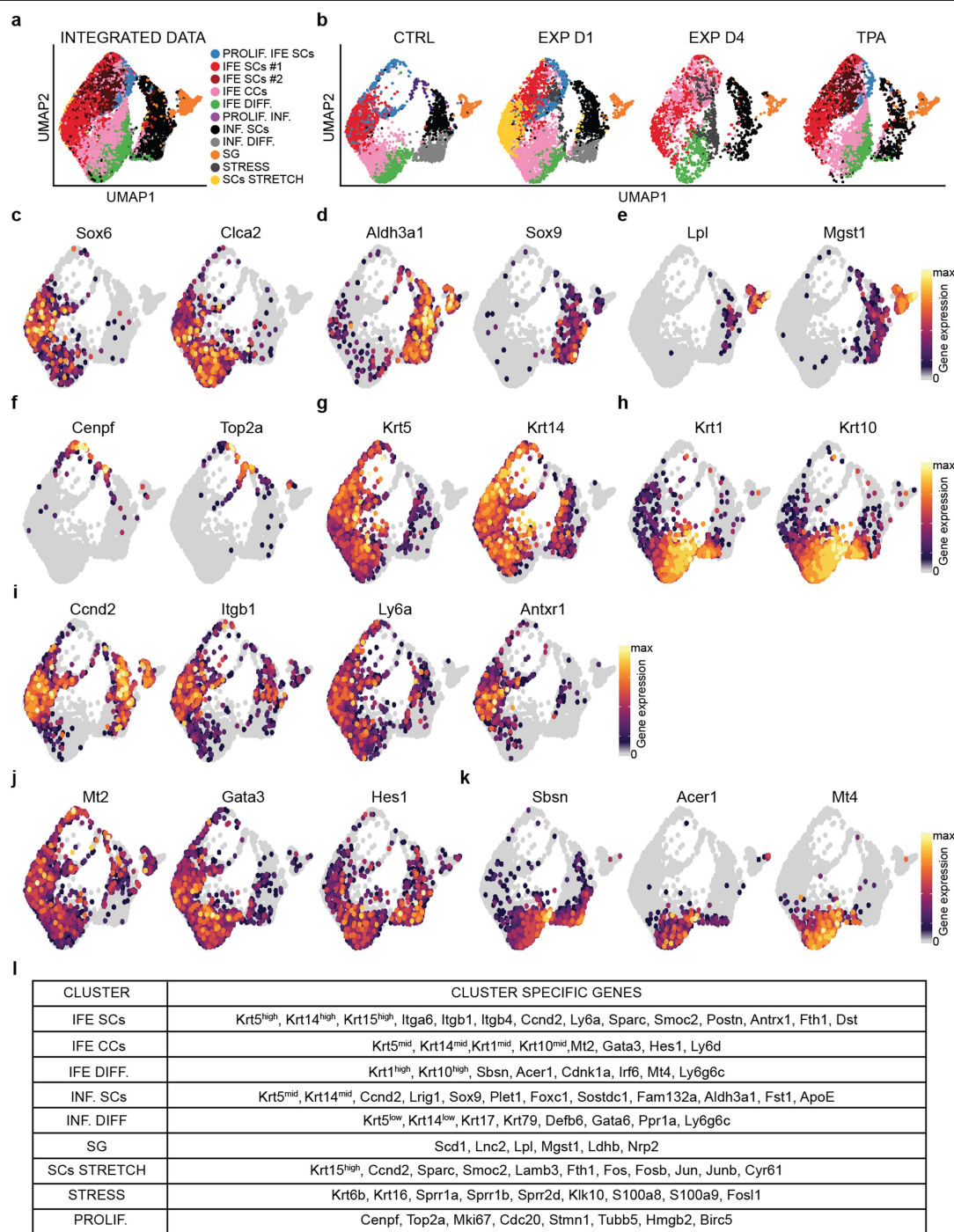
Extended Data Fig. 6 | Single-cell RNA sequencing clustering analysis.
**a**, UMAP graphic representation of the CTRL, EXP D1, EXP D4 and TPA single-cell RNA-seq data, showing the graph-based clustering results annotated by cell type. The proliferating IFE stem cells (PROLIF. IFE SCs) are in light blue, the IFE stem cells cluster are in red (IFE SCs#1) and dark red (IFE SCs#2), the IFE committed cells (IFE CCs) cluster is in pink and the differentiated IFE cells (IFE DIFF.) are in green. The differentiated cells from the infundibulum (INF. DIFF.) are in grey, the stem cells of the infundibulum (INF. SCs.) are in black, the proliferating cells of the infundibulum (PROLIF. INF.) are in plum and the sebaceous gland cluster (SG) is in orange. The IFE stress cells (STRESS) are in dark grey and the cluster of stem cells stretch (SCs STRETCH) in yellow. n = 16,651 cells. **b**, UMAP of the different samples (CTRL, EXP D1, EXP D4,

TPA) using the same integrated projection. n = 4,659 cells CTRL, n = 4,934 cells EXP D1, n = 2,716 cells EXP D4, n = 4,342 cells TPA. **c–k**, UMAP plot of the CTRL sample colored by normalized gene expression values for genes identifying the IFE (**c**) versus infundibulum (**d**), the sebaceous gland (**e**) and the proliferating cells (**f**). Undifferentiated (**g**) and more differentiated cells (**h**) in the IFE identified the SCs cluster (**i**), the CCs cluster (**j**) and the differentiated stage (**k**). Gene expression is visualized as a colour gradient going from grey to yellow with grey as indicator of no expression (that is, expression values below or equal to the 50th percentile for that sample) and yellow as indicator of maximal expression. **c–k**, n = 16,651 cells. **l**, Table showing the specific marker genes used to annotate the different clusters.

Article
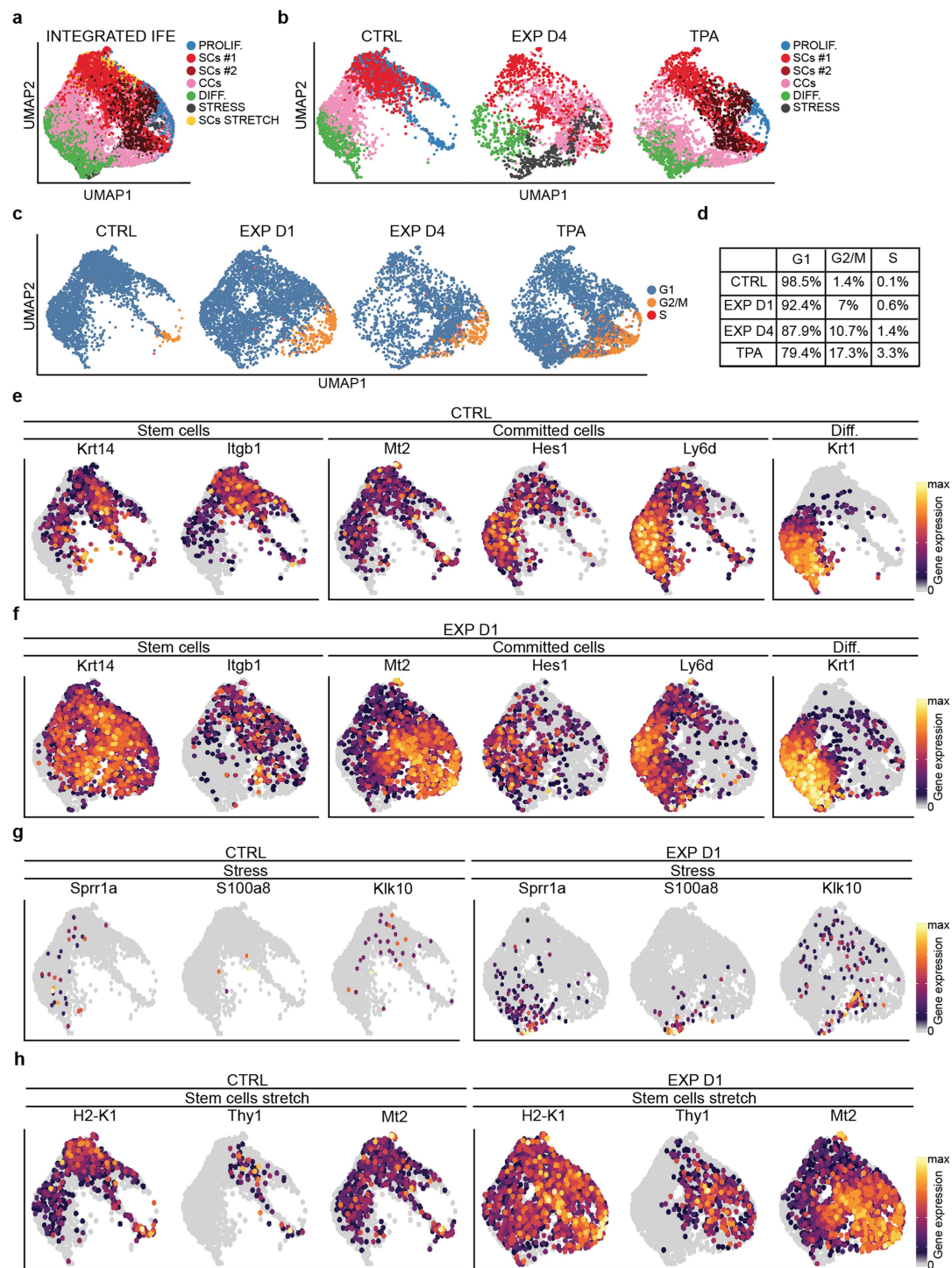
Extended Data Fig. 7 | Single-cell RNA sequencing clustering analysis on the IFE cells. a, Integrated UMAP graphic representation of the IFE cells in CTRL, EXP D1, EXP D4 and TPA single-cell RNA-seq data, showing the graph-based clustering results annotated by cell type. The proliferating stem cells (PROLIF.) are in light blue, the stem cells clusters are in red and dark red (SCs#2), the committed cells (CCs) cluster is in pink and the differentiated cells (DIFF.) are in green. The stress cells (STRESS) are in dark grey and the cluster of stem cells stretch (SCs STRETCH) in yellow. $n = 12,747$ cells. **b**, UMAP of the different samples (CTRL, EXP D1, EXP D4, TPA). **c**, Predicted cell-cycle phases assigned using the *cyclone* function from *scran* tool and visualized in the UMAP. Cells in G1 are in light blue, cells in G2/M are in orange and cells in S phase are in red. **b**–**d**, $n = 3,142$ cells CTRL, $n = 3,756$ cells EXP D1, $n = 2,145$ cells EXP D4, $n = 3,704$ cells TPA. **d**, Percentage of cells in the different cycling phase calculated on the total number of cells. **e**–**h**, UMAP plot colored by normalized gene expression values for the indicated gene and in the indicated sample. Gene expression is visualized as a colour gradient going from grey to yellow with grey as indicator of no expression and yellow as indicator of maximal expression. $n = 3,142$ cells CTRL, $n = 3,756$ cells EXP D1.
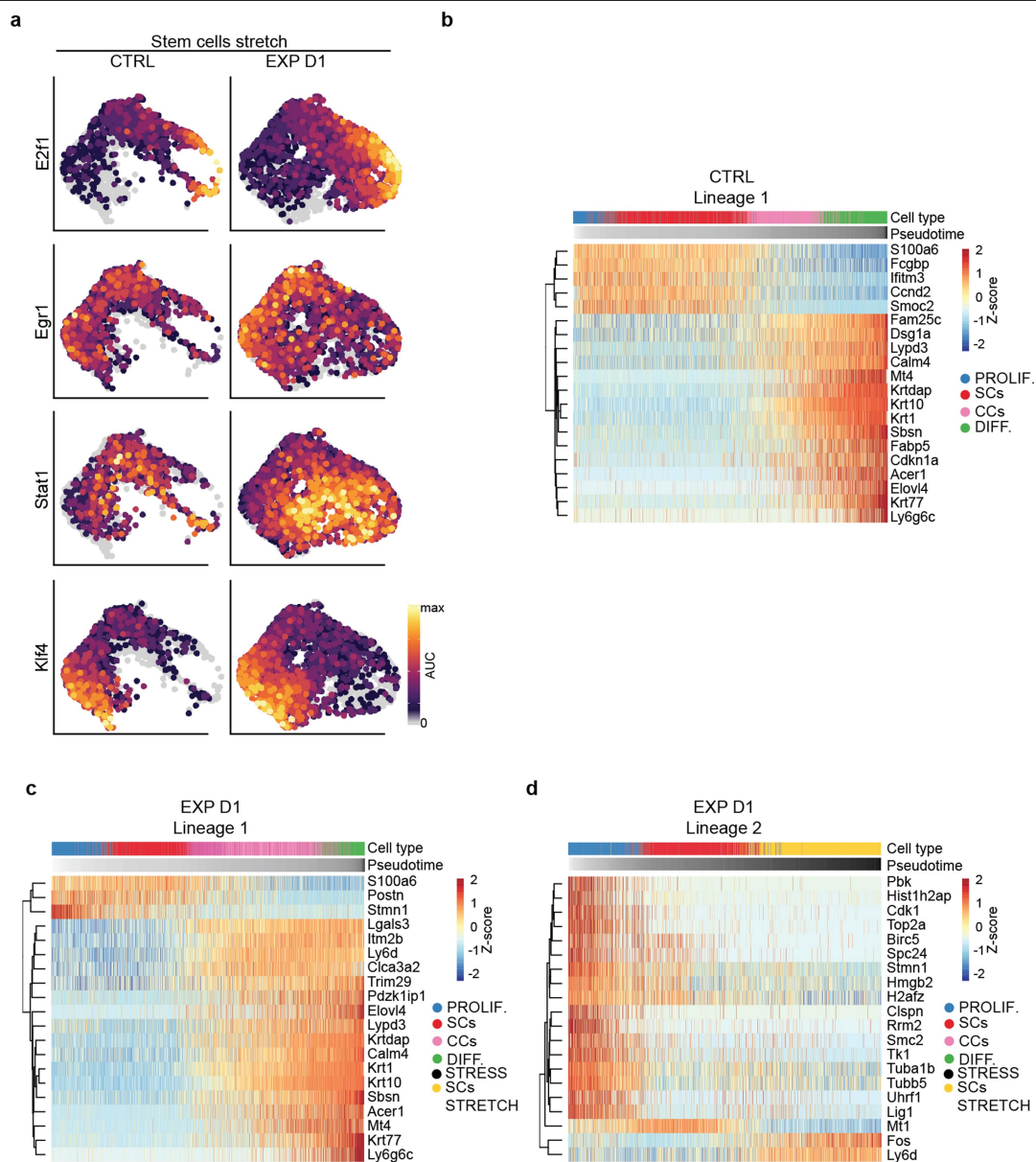
Extended Data Fig. 8 | Pseudotime analysis for single-cell RNA sequencing. a, UMAP plots coloured by the degree of regulon activation for TFs differentially activated (AUC rank-sum test FDR corrected p-value <0.05) in the different conditions. Colour scaling represents the normalized AUC value of target genes in the regulon being expressed as computed by SCENIC. **b**, Heat map representation of the top 20 gene expression changes along the inferred pseudotime trajectory computed with Slingshot for the CTRL IFE. **c**, Heat map representation of the top 20 gene expression changes along the inferred pseudotime homeostatic trajectory computed with Slingshot for the EXP D1 IFE. **d**, Heat map representation of the top 20 gene expression changes along the inferred pseudotime trajectory computed with Slingshot characterizing the stress state for the EXP D1 IFE. **b**–**d**, Columns represent cells ordered by their position along the pseudotime trajectory; rows represent genes whose expression profiles show highest correlation (FDR-correted p-value <0.01) with the pseudotime variable, calculated using a generalized additive model (GAM). The colour scaling of the cells represents the normalized expression value of a gene in a particular cell, scaled by Z-score. **a**–**d**, $n = 3,142$ cells CTRL, $n = 3,756$ cells EXP D1.
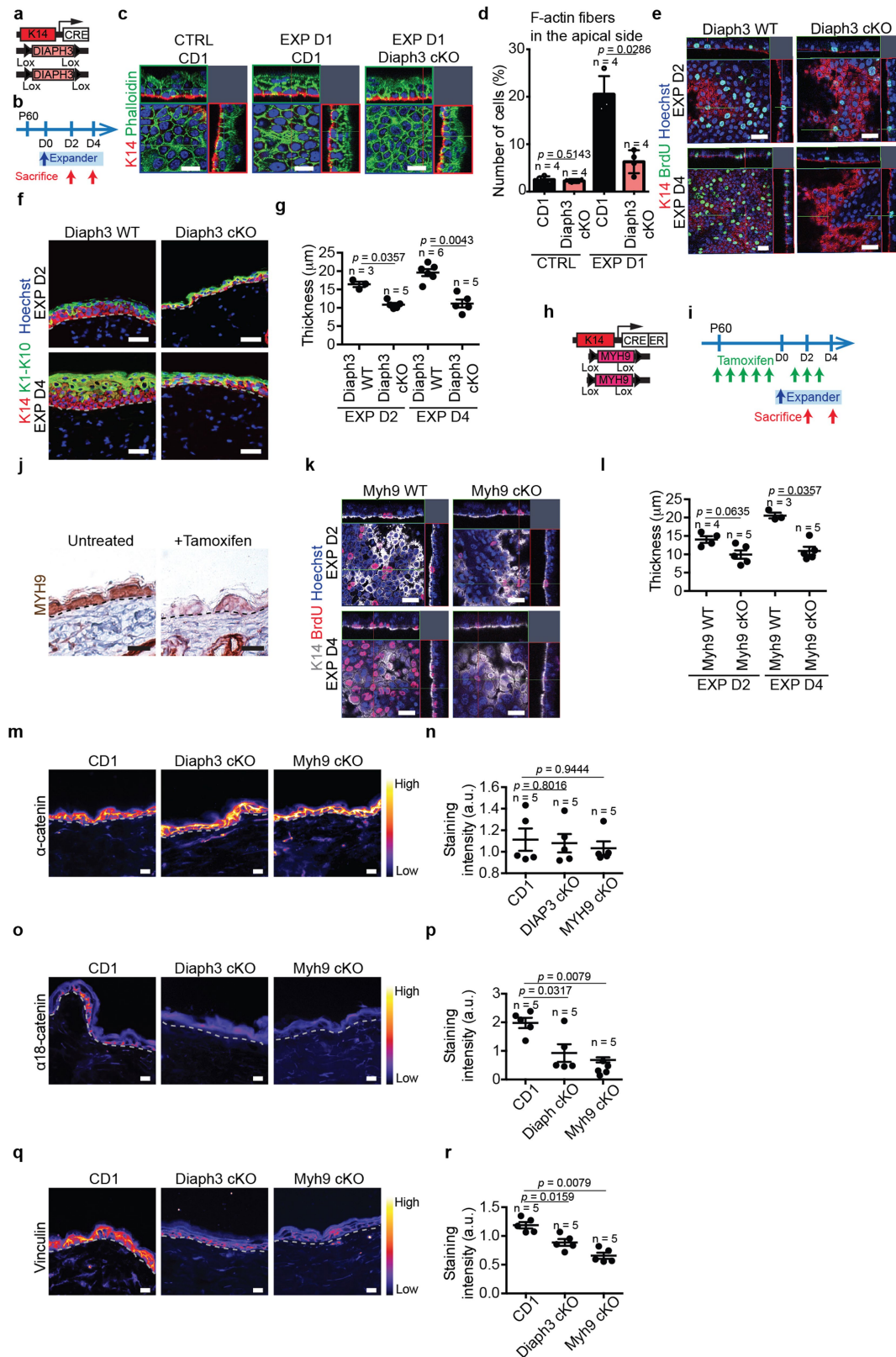
Extended Data Fig. 9 | See next page for caption.

Extended Data Fig. 9 | Cell contractility in stretch-mediated tissue expansion. a, Scheme of the genetic strategy to delete *Diaph3* in the epidermis. **b**, Protocol to delete *Diaph3* during stretch-mediated tissue expansion. **c**, Orthogonal views of confocal analysis of immunostaining for K14 (red) marking basal cells and Phalloidin (green) to visualize F-actin and Hoechst for nuclei (blue) in whole mounts of IFE in CTRL from a CD1 mouse, EXP D1 from a CD1 or *Krt14-cre-DIAPH3fl/fl* (*Diaph3* cKO) mouse. Scale bars, 10 μm. **d**, Percentage of cells with F-actin fibres in the apical side of basal cells related to **c** (*n* = 4 mice per condition). **e**, Orthogonal views of confocal analysis of immunostaining for K14 (red) marking basal cells, BrdU (green) and Hoechst for nuclei (blue) in whole mounts of IFE from *Krt14-cre-DIAPH3fl/+* (*Diaph3* WT) and *Krt14-cre-DIAPH3fl/fl* (*Diaph3* cKO) mice during expansion. Scale bars, 20 μm. Epidermal *Diaph3* cKO were born at a Mendelian ratio and did not present obvious pathological phenotypes. *n* = 3 independent experiments. **f**, Immunostaining for the basal marker K14 (red) and the suprabasal markers K1 and K10 (green) in *Diaph3* WT and *Diaph3* cKO mice in EXP D2 and EXP D4. Scale bars, 20 μm. **g**, Epidermal thickness of *Diaph3* WT and *Diaph3* cKO mice in EXP D2 and EXP D4 (three measurements taken with ImageJ on two sections per mouse, *n* = at least 3 mice for the different conditions). **h**, Scheme of the genetic strategy to delete *Myh9* in the epidermis. **i**, Protocol to delete *Myh9* during stretch-mediated tissue expansion. **j**, Immunohistochemistry for MYH9 in untreated and Tamoxifen induced *Krt14-creER-MYH9fl/fl* mice. Scale bars, 20 μm. *n* = 3 independent experiments. **k**, Orthogonal views of confocal analysis of immunostaining for K14 (white), BrdU (red) and Hoechst for nuclei (blue) in whole mounts of IFE in *Myh9* WT and *Myh9* cKO mice during expansion. Scale bars, 20 μm. **l**, Epidermal thickness of *Myh9* WT and *Myh9* cKO mice in EXP D2 and EXP D4 (three measurements taken with ImageJ on two sections per mouse, *n* = at least 3 mice for the different conditions). **m–r**, Analysis of adherens junctions in *Diaph3* cKO and *Myh9* cKO mice. **m**, **o**, **q**, Representative images of adherens junction (AJ) component α-catenin (**m**), the α18 tension sensitive form of α-catenin (α18-catenin) (**o**) and Vinculin (**q**), colour-coded for the signal intensity with ImageJ. Protein expression is visualized as a colour gradient going from black to yellow, with black as indicator of no expression and yellow as indicator of maximal expression. Dashed lines indicate the basal lamina. Scale bars, 10 μm. **n**, **p**, **r**, Quantification of the average integrated density signal for α-catenin (**n**), α18-catenin (**p**) and Vinculin (**r**). Each data point is the average of 3 sections per mouse (*n* = 5 mice per condition). **d**, **g**, **l**, **n**, **p**, **r**, Two-tailed Mann–Whitney test, mean + s.e.m.

Extended Data Fig. 10 | See next page for caption.
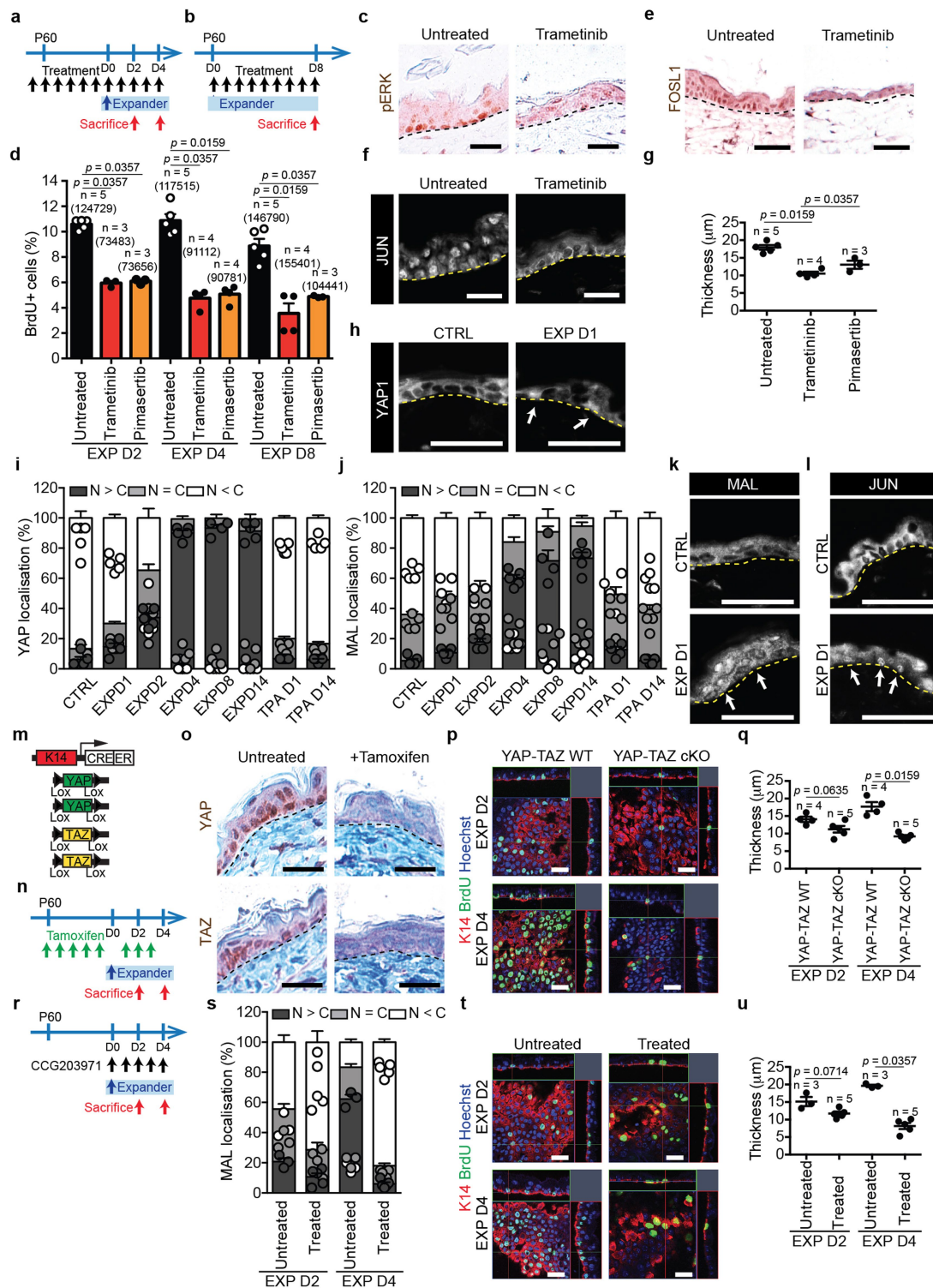
Extended Data Fig. 10 | MEK/ERK/AP1, YAP-TAZ and MAL/SRF regulate stretch-mediated proliferation. a, **b**, Protocol for Trametinib or Pimasertib treatment in CD1 mice operated to place the expander and scarified at D2, D4 (**a**) and D8 (**b**) after surgery. **c**, Immunohistochemistry for pERK on paraffin sections of epidermis form CD1 mice untreated or treated with the indicated drug at EXP D2. **d**, Quantification of the proportion of BrdU positive cells during expansion at the indicated time point in CD1 mice untreated or treated with Trimatenib or Pimasertib (*n* = at least 3 mice per condition as indicated, total number of cells analysed indicated in parentheses). **e**, **f**, Immunohistochemistry for FOSL1 (**e**) and immunofluorescence for JUN (**f**) on sections of epidermis from CD1 mice untreated or treated with the indicated drug at EXP D2. **g**, Epidermal thickness measured with ImageJ on tissue sections at EXP D8 in CD1 mice untreated or treated with the indicated drug (*n* = 5 mice untreated, *n* = 4 mice Trametinib, *n* = 3 mice Pimasertib, 3 measurements on at least 2 sections per mouse). **h**, Immunostaining (white) for YAP1 on skin sections in the control and in EXP D1. White arrows indicate nuclear localization. **i**, Quantification of YAP1 subcellular localization, bars and error bars represent the mean and s.e.m. Nuclear (N) > Cytosplasm (C), more YAP1 in nucleus than in cytoplasm, N = C, similar level of YAP1 in nucleus than in cytoplasm, N < C, less YAP1 in nucleus than in cytoplasm (*n* = 150 cells for all samples except *n* = 120 for EXP D8). **j**, Quantification of MAL subcellular localization, presented as mean and s.e.m. N > C, more MAL in nucleus than in cytoplasm, N = C, similar level of MAL in nucleus than in cytoplasm, N < C, less MAL in nucleus than in cytoplasm (*n* = 150 cells for all samples except *n* = 120 for EXP D8). **k**, **l**, Immunostaining (white) for MAL (**k**) and JUN (**l**) on skin sections in the control and in EXP D1. White arrows indicate nuclear localization.

m, **n**, Scheme of the genetic strategy to delete YAP-TAZ in the epidermis (**m**) and protocol to delete YAP and TAZ in stretch-mediated tissue expansion (**n**). **o**, Immunohistochemistry for YAP (top) and TAZ (bottom) in *Krt14-creER-YAP-TAZfl/fl* mice before and after Tamoxifen administration. **p**, Orthogonal views of confocal analysis of immunostaining for K14 (red) marking basal cells, BrdU (green) and Hoechst for nuclei (blue) in whole mounts of IFE in *YAP-TAZfl/fl* (*YAP-TAZ* WT) or *Krt14-creER-YAP-TAZfl/fl* (*YAP-TAZ* cKO) mice at the indicated time point following expansion. **q**, Epidermal thickness of *YAP-TAZ* WT and *YAP-TAZ* cKO mice in EXP D2 and EXP D4 (three measurements taken with ImageJ on two sections per mouse, *n* = at least 4 mice per condition). **r**, Protocol to inhibit MAL with the CCG203971 small molecule during stretch-mediated tissue expansion. **s**, Quantification of MAL subcellular localization in EXP D2 and EXP D4 mice treated or not with the MAL inhibitor. N > C, more MAL in nucleus than in cytoplasm, N = C, similar level of MAL in nucleus than in cytoplasm, N < C, less MAL in nucleus than in cytoplasm (*n* = 150 cells per condition). Data are presented as mean and s.e.m. **t**, Orthogonal views of confocal analysis of immunostaining for K14 (red) marking basal cells, BrdU (green) and Hoechst for nuclei (blue) in whole mounts of IFE in mice treated with the MAL inhibitor or with vehicle control (untreated) at the indicated time point following expansion. **u**, Epidermal thickness of CD1 mice in EXP D2 and EXP D4 treated or not with the MAL inhibitor (three measurements taken with ImageJ on two sections per mouse, *n* = 3 for untreated mice, *n* = 5 for treated animals). **c**, **e**, **f**, **h**, **k**, **l**, **o**, **p**, **t**, Scale bars, 20 µm. *n* = 3 independent experiments. **c**, **e**, **f**, **h**, **k**, **l**, **o**, Dashed lines delineate the basal lamina. **d**, **g**, **q**, **u**, Two-tailed Mann–Whitney test, mean + s.e.m.
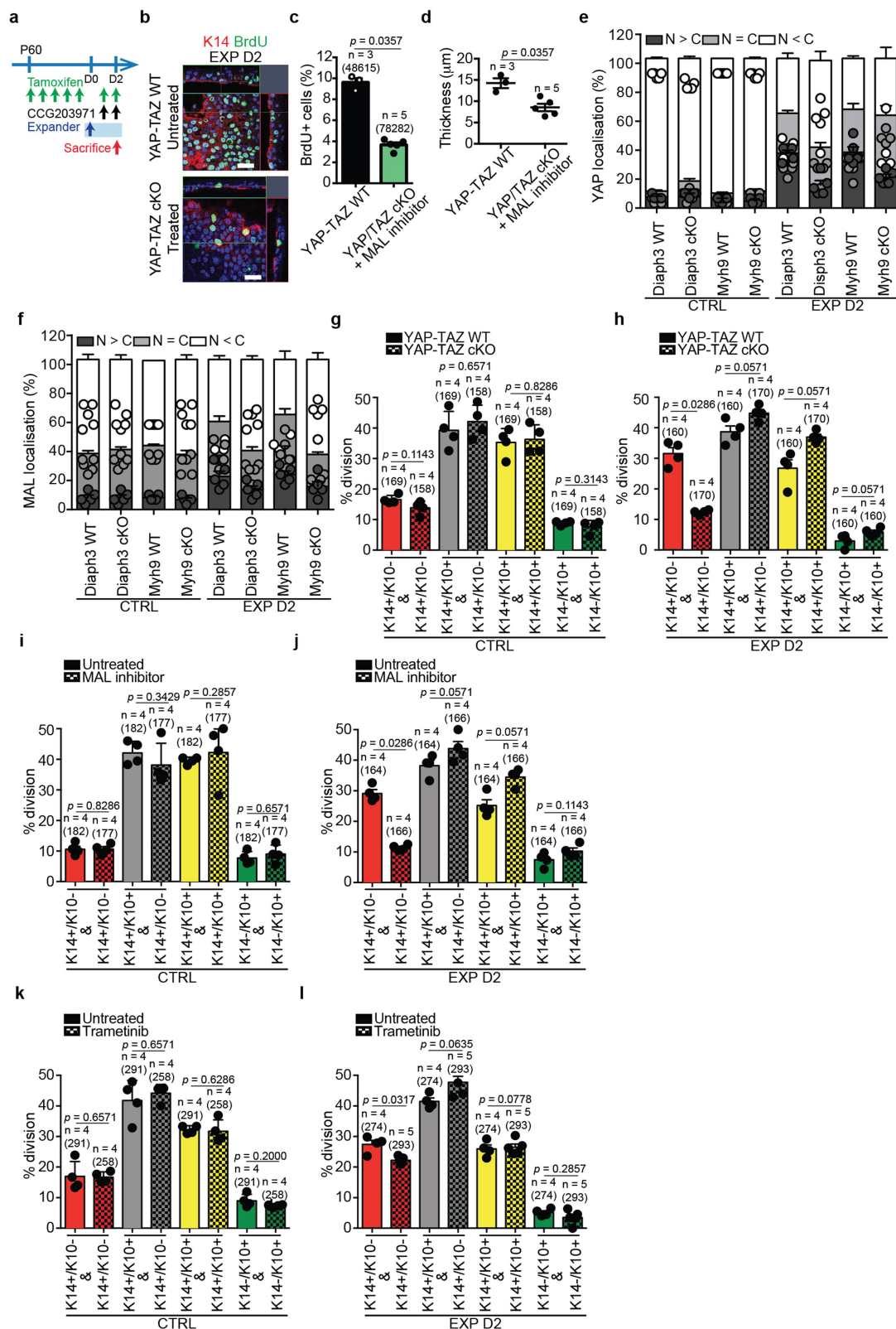
Extended Data Fig. 11 | See next page for caption.

Extended Data Fig. 11 | Pathways associated with stretch-mediated tissue expansion. a, Protocol used to delete YAP and TAZ and to inhibit MAL with CCG203971 treatment in *Krt14-creER-YAP-TAZfl/fl* mice in EXP D2. **b**, Orthogonal views of immunostaining for K14 (red) to mark basal cells, BrdU (green) and Hoechst for nuclei (blue) on whole mounts of IFE in *YAP-TAZ* WT untreated mice and *YAP-TAZ* cKO mice treated with the MAL inhibitor at 2 days after the expander placement. Scale bars, 20 μm. **c**, Proportion of BrdU positive cells in untreated *YAP-TAZ* WT mice (48,615 cells from 3 mice) and in *YAP-TAZ* cKO mice treated with the MAL inhibitor (78,282 cells from 5 mice). Two-tailed Mann–Whitney test, mean + s.e.m. **d**, Epidermal thickness of *YAP-TAZ* WT untreated ($n = 3$) and *YAP-TAZ* cKO treated with the MAL inhibitor in EXP D2 ($n = 5$), three measurements taken with ImageJ on two sections per mouse. Two-tailed Mann–Whitney test, mean + s.e.m. **e**, **f**, Quantification of YAP1 (**e**) and MAL (**f**) subcellular localization, presented as mean and s.e.m. in CTRL and EXP D2. N > C, more protein in nucleus than in cytoplasm, N = C, similar level of protein in nucleus than in cytoplasm, N < C, less protein in nucleus than in cytoplasm ($n = 150$ cells per condition). **g**, **h**, Percentage of the type of divisions in CTRL (**g**) and EXP D2 (**h**) in *YAP-TAZ* WT mice and *YAP-TAZ* cKO mice based on the short-term BrdU tracing and staining as in Extended Data Fig. 4h. **i**, **j**, Percentage of the type of divisions in CTRL (**i**) and EXP D2 (**j**) in Untreated mice and with MAL inhibitor based on the short-term BrdU tracing and staining as in Extended Data Fig. 4h. **k**, **l**, Percentage of the type of divisions in CTRL (**k**) and EXP D2 (**l**) in Untreated mice and with Trametinib based on the short-term BrdU tracing and staining as in Extended Data Fig. 4h. **g**–**l**, The number of counted divisions is indicated in parenthesis from n = number of mice. Two-tailed Mann–Whitney test, mean + s.e.m.

Article
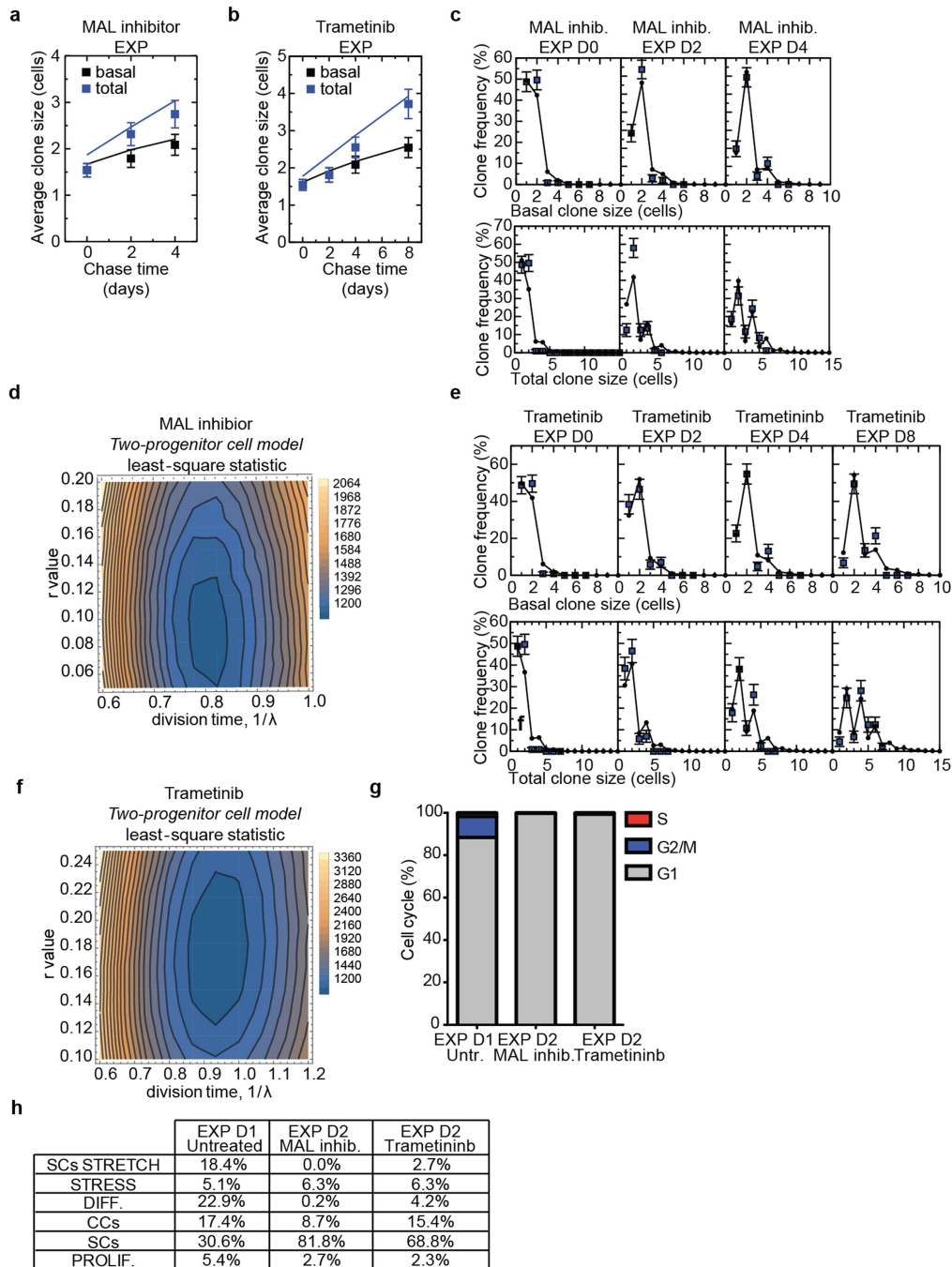
Extended Data Fig. 12 | Single-cell data analysis after MEK and MAL inhibition. a, Average size of persisting clones in mice treated with MAL inhibitor during expansion, based on the basal (black) and total (blue) cell content. Points show data and lines denote the results from the fit to the two-compartment model (see main text and Methods). D0: n = 115 clones from 7 mice; D2: n = 86 clones from 3 mice; D4: n = 83 clones from 3 mice. **b**, Average size of persisting clones in mice treated with Trametinib during expansion, based on the basal (black) and total (blue) cell content. Points show data and lines denote the results from the fit to the two-compartment model (see main text and Methods). D0: n = 115 clones from 7 mice; D2: n = 84 clones from 3 mice; D4: n = 80 clones from 4 mice; D8: n = 81 clones from 3 mice. **c**, Fit of the model to the clone size distribution during expansion upon MAL inhibition with $1/\lambda$ = 3.8 days and r = 0.08. D0: n = 115 clones from 7 mice; D2: n = 86 clones from 3 mice; D4: n = 83 clones from 3 mice. **d**, Least-square values indicate the sensitivity of the fit parameters in **c**. **e**, Fit of the model to the clone size distribution during expansion upon Trametininb treatment with $1/\lambda$ = 4.3 days and r = 0.17. D0: n = 115 clones from 7 mice; D2: n = 84 clones from 3 mice; D4: n = 80 clones from 4 mice; D8: n = 81 clones from 3 mice. **f**, Least-square values indicate the sensitivity of the fit parameters in **e**. **g**, Predicted cell-cycle phases assigned using the *cyclone* function from *scran* tool of EXP D1 Untreated IFE, EXP D2 IFE treated with the MAL inhibitor and EXP D2 IFE treated with Trametinib. Cells in G1 are in grey, cells in G2/M are in blue and cells in S phase are in red. The percentage of cells in the different cycling phases is calculated on the total number of cells. **h**, Table showing the values of the percentage of the different cellular clusters in Fig. 4j, k. **a**, **b**, Mean + s.d. **c**, **e**, Mean + s.e.m.

nature research

Corresponding author(s): Cédric Blanpain, Benjamin D. Simons

Last updated by author(s): 16/06/2020

Reporting Summary

Nature Research wishes to improve the reproducibility of the work that we publish. This form provides structure for consistency and transparency in reporting. For further information on Nature Research policies, see Authors & Referees and the Editorial Policy Checklist.

Please do not complete any field with "not applicable" or n/a. Refer to the help text for what text to use if an item is not relevant to your study.
For final submission: please carefully check your responses for accuracy; you will not be able to make changes later.

Statistics

For all statistical analyses, confirm that the following items are present in the figure legend, table legend, main text, or Methods section.

n/a	Confirmed	
☐	☒	The exact sample size (*n*) for each experimental group/condition, given as a discrete number and unit of measurement
☐	☒	A statement on whether measurements were taken from distinct samples or whether the same sample was measured repeatedly
☐	☒	The statistical test(s) used AND whether they are one- or two-sided *Only common tests should be described solely by name; describe more complex techniques in the Methods section.*
☒	☐	A description of all covariates tested
☒	☐	A description of any assumptions or corrections, such as tests of normality and adjustment for multiple comparisons
☐	☒	A full description of the statistical parameters including central tendency (e.g. means) or other basic estimates (e.g. regression coefficient) AND variation (e.g. standard deviation) or associated estimates of uncertainty (e.g. confidence intervals)
☒	☐	For null hypothesis testing, the test statistic (e.g. *F*, *t*, *r*) with confidence intervals, effect sizes, degrees of freedom and *P* value noted *Give P values as exact values whenever suitable.*
☒	☐	For Bayesian analysis, information on the choice of priors and Markov chain Monte Carlo settings
☒	☐	For hierarchical and complex designs, identification of the appropriate level for tests and full reporting of outcomes
☒	☐	Estimates of effect sizes (e.g. Cohen's *d*, Pearson's *r*), indicating how they were calculated

Our web collection on statistics for biologists contains articles on many of the points above.

Software and code

Policy information about availability of computer code

Data collection	Microscope: Axio Imager M1, Axiovision 4.8.2, Zeiss. Confocal: LSM 780, Zeiss, ZEN2012, Zeiss. Flow cytometry: FACSAria, FACS DiVa, BD Biosciences,8.0.1, 2014, firmware 1.4, CST 3.0.1, PLA 2.0. TEWL: TM210,Courage and Khazaka. TEM: JEOL JEM1400. qPCR: Light Cycler 96 (Roche). Single-cells: Chromium Single Cell 3' (V2-chemistry, PN-120232, 10X Genomics), 10X Chromium controller (10x Genomics).
Data analysis	Microscope and confocal: ZEN 2012 (Zeiss), ImageJ (1.46r). Statistical analysis: Excel (14.4.3), GraphPad Prism (7.00). ATAC-seq: R software (v3.5.1), Bowtie2 (2.2.6), MACS2 (2.1.0.20151222), GREAT (3.0.0), HOMER (10). Single-cells analysis: 10X Genomics, CellRanger (2.1.1) , R package (1.10.0), R package (1.10.2), Seurat R package (3.1.1). Slingshot (1.1.0), SCENIC.

For manuscripts utilizing custom algorithms or software that are central to the research but not yet described in published literature, software must be made available to editors/reviewers. We strongly encourage code deposition in a community repository (e.g. GitHub). See the Nature Research guidelines for submitting code & software for further information.

Data

Policy information about availability of data

All manuscripts must include a data availability statement. This statement should provide the following information, where applicable:

- Accession codes, unique identifiers, or web links for publicly available datasets
- A list of figures that have associated raw data
- A description of any restrictions on data availability

Data associated with this study have been deposited in the NCBI Gene Expression Omnibus under accession number GSE126231, GSE126734 and GSE146637 respectively for the microarray, ATAC-seq and single-cell RNA-seq. Data supporting the findings of this study are available within the article (and its Supplementary Information files). Source data behind Figures 1-4 Extended Data Figures 1-12 are available within the manuscript files.

Field-specific reporting

Please select the one below that is the best fit for your research. If you are not sure, read the appropriate sections before making your selection.

☒ Life sciences ☐ Behavioural & social sciences ☐ Ecological, evolutionary & environmental sciences

For a reference copy of the document with all sections, see nature.com/documents/nr-reporting-summary-flat.pdf

Life sciences study design

All studies must disclose on these points even when the disclosure is negative.

Sample size	No statistical methods were used to predetermine sample size. All experiments were repeated at least three times. In microarray, TPA was repeated twice with reproducible results. Single-cell: the results for each mouse were grouped and analyzed together in all conditions. The number of animals has been reduced for ethical reasons.
Data exclusions	No animals were excluded from the analysis.
Replication	All experiments were repeated at least three times (3 biological independent experiments/mice) showing similar results, except for microarray analysis for which one condition experiment (TPA) was repeated twice (2 biological independent experiments/mice) and single cell for which we analysed one mouse per condition (1 biological independent experiment/mouse). All attempts at replication were successfull and are shown, n is described in legends.
Randomization	The experiments were not randomized. The mice included in this study were selected according to their correct genotype. The mice received tamoxifen injection/s when they were 2 months old. Sex-specific differences were minimized by including similar number of male and female animals.
Blinding	The investigators were not blinded to allocation during experiments and outcome assessment. Blinding was not possible as the same investigator processed the animals and analysed the data.

Reporting for specific materials, systems and methods

We require information from authors about some types of materials, experimental systems and methods used in many studies. Here, indicate whether each material, system or method listed is relevant to your study. If you are not sure if a list item applies to your research, read the appropriate section before selecting a response.

Materials & experimental systems

n/a	Involved in the study
☐	☒ Antibodies
☒	☐ Eukaryotic cell lines
☒	☐ Palaeontology
☐	☒ Animals and other organisms
☒	☐ Human research participants
☒	☐ Clinical data

Methods

n/a	Involved in the study
☒	☐ ChIP-seq
☐	☒ Flow cytometry
☒	☐ MRI-based neuroimaging

Antibodies

Antibodies used	For immunofluorescence and ISH the following primary antibodies were used: anti-B4-integrin (Rat, 1:200, BD, clone346-11A, ref.553745, lot.5239648), anti-Keratin10 (rabbit, 1/3000, Covance, ref.PRB-159P-0100), anti-Keratin1 (rabbit, 1/3000, Covance, ref.PRB-165P-0100), anti-Keratin-14 (rabbit, 1/3000, Thermofisher), anti-BrdU (mouse, 1/200, BD, clone 3D4,ref. 560209, lot.4293550), anti-MAL (rabbit,1/200, Sigma, ref.HPA030782,lot.C106712), anti-c-JUN (rabbit, 1/200; Proteintech, 24909-1-AP); anti-p63 (rabbit, 1/100 Abcam, ab124762); anti-KLF4 (rabbit, 1/100 Abcam, ab129473); anti-pSTAT3 (rabbit, 1/100 Cell signaling, 9145); anti-YAP1 (rabbit, 1/100 Proteintech, 13584-1-AP); rabbit anti-YAP (1:200, Santa Cruz Biotechnology, sc-15407), rabbit anti-TAZ (1:100, Sigma-Aldrich, HPA007415), rabbit anti-cFOS (1:100, Proteintech, 26192-1-AP), rabbit anti-MYH9 (1:500, Sigma, HPA001644), rabbit anti-pERK (1:200, Cell signaling, 4370S), anti-FOSL1 (1:500, Santa Cruz Biotechnology, sc-28310), anti-β-catenin (mouse, 1:1000 Abcam ab6301), anti-α-catenin (rabbit, 1:1000 Sigma, C2081); anti-α18-catenin (rat monoclonal, 1:20000) was a generous gift form Akira Nagafuchi, Kumamoto University; anti-Vinculin (mouse, 1:200 Millipore MAB3574); anti-p120-catenin (rabbit, 1:1000 Invitrogen PA5-82545); anti-E-cadherin (rat, 1:500, ebioscience 14-3249-82); anti-ZO-1(rabbit, 1:200 Invitrogen 61-7300); anti-Claudin-1 (rat, 1:100Thermo Scientific 51-9000); anti-Paxillin (rabbit, 1:100 Abcam 32084); anti-CD45 (rat, 1:500, BD Biosciences 553081); anti-CD68 (rabbit, 1:100 Abcam ab125212); anti-SOX6 (rabbit, 1:400 Sigma HPA001923); anti-NFIB (rabbit, 1:200 Sigma HPA003956). The following secondary antibodies were used: anti-rabbit, anti-rat, anti-goat, anti-chicken, anti-mouse conjugated to AlexaFluor488 (Molecular Probes) and to rhodamine Red-X and Cy5 (JacksonImmunoResearch).
Validation	As positive control for immunostaining, tissues with known expression of the marker were used on mouse sections. As negative control, for immunostaining, staining omitting the primary antibody was performed.

Animals and other organisms

Policy information about <u>studies involving animals</u>; <u>ARRIVE guidelines</u> recommended for reporting animal research

Laboratory animals	K14CREER and K14CRE transgenic mice were kindly provided by E. Fuchs, Rockefeller University, USA. Rosa-Confetti mice were provided by H. Clevers. YAPfl/fl and TAZfl/fl mice were obtained from Georg Halder (KU Leuven) who received them from Randy Johnson at the MD Anderson Cancer Center, Houston. Diap3fl/fl mice were obtained from Fadel Tissil (UCL) and MYH9fl/fl mice were a kindly gift from Sara Wickström (University of Helsinki). Rosa26-mT/mG mice were provided form Isabelle Migeotte (Université Libre de Bruxelles). Mice included in this study were from mixed genetic background. Female and male animals have been used for all experiments and equal animal gender ratios have been respected in the majority of the analysis. Mice were included in the study when they were 2 months old when the tamoxifen was administred.
Wild animals	No wild animals were used in this study.
Field-collected samples	No field-collected samples were used in this study.
Ethics oversight	Mice colonies were maintained in a certified animal facility in accordance with European guidelines. The experiments were approved by the local ethical committee (CEBEA) under protocols #604 and #605.The study is compliant with all relevant ethical regulations regarding animal research.

Note that full information on the approval of the study protocol must also be provided in the manuscript.

Flow Cytometry

Plots

Confirm that:

◻ The axis labels state the marker and fluorochrome used (e.g. CD4-FITC).

◻ The axis scales are clearly visible. Include numbers along axes only for bottom left plot of group (a 'group' is an analysis of identical markers).

◻ All plots are contour plots with outliers or pseudocolor plots.

◻ A numerical value for number of cells or percentage (with statistics) is provided.

Methodology

Sample preparation	The mice were shaved with an electric shaver, the back skin was dissected from the mice, fat and underlying subcutis were removed with a scalpel. The samples were placed in 0,25% Trypsin (Gibco, Thermo Fisher Scientific) in DMEM-Dulbecco's modified Eagle's medium (Gibco, Thermo Fisher Scientific) and 2mM EDTA (Thermo Fisher Scientific) overnight at 4°C. The epidermis was separated form the dermis and the trypsin was neutralized by adding DMEM medium supplemented with 2% Chelex Fetal Calf Serum (FCS). Samples were filtrated on 70 and 40µm filter (Falcon). Single cells suspension were incubated in 2% FCS/PBS with primary antibodies for 30 min on ice, protected from the light, with shaking every 10 min. Primary antibodies were washed with 2% FCS/PBS and cells incubated for 30 min in APC-conjugated streptavidin (BD Biosciences), on ice, with shaking every 10 min. Living epidermal cells were gated by forward scatter, side scatter and negative staining for Hoechst dye. Basal IFE and infundibulum cells were stained using PE-conjugated anti-α6-integrin (clone GoH3; 1/200, ebioscience) and bulge cells were stained with biotinylated CD34 (clone RAM34; 1:50, BD Biosciences). Basal cells from the interfollicular epidermis were targeted using CD34 negative and α6 integrin positive gating. The geometric mean fluorescence intensity of Itgβ1 (FITC-coniugated anti-β1-integrin, 1:100, BD Bioscience 555005) and Itga2 (PE-coniugated anti-α2-integrin, 1:100, BD Bioscience 553858) was measured on the α6-integrinhigh/CD34neg population.
Instrument	FACSAria III (BD Bioscience)
Software	FACSDiva Software 8.0.1 (BD Bioscience)
Cell population abundance	The proportion of the relevant cell populations is depicted in Extended Data Fig.3a
Gating strategy	Living cells were selected by forward scatter, side scatter, doublets discrimination and by Hoechst dye exclusion. Basal epidermal cells were selected based on the expression of Integrin-alhap6-high-PE and Cd34-APC negative.

◻ Tick this box to confirm that a figure exemplifying the gating strategy is provided in the Supplementary Information.